Title: Enhancing purification efficiency of affinity functionalized composite agarose micro beads using Fe_3O_4 nanoparticles

Author: S. Amiri M.R. Mehrnia F. Pourasgharian Roudsari

PII: S1570-0232(16)31315-0
DOI: http://dx.doi.org/doi:10.1016/j.jchromb.2016.11.035
Reference: CHROMB 20363

To appear in: *Journal of Chromatography B*

Received date: 18-7-2016
Revised date: 12-11-2016
Accepted date: 23-11-2016

Please cite this article as: S.Amiri, M.R.Mehrnia, F.Pourasgharian Roudsari, Enhancing purification efficiency of affinity functionalized composite agarose micro beads using Fe3O4 nanoparticles, Journal of Chromatography B http://dx.doi.org/10.1016/j.jchromb.2016.11.035

Highlights

- Investigating effects of magnetic nanoparticles on adsorption properties of beads
- Specific surface area of magnetic beads is significantly more than nonmagnetic ones
- Cibacron Blue F3GA (CB) was used as affinity ligand.
- CB density on magnetic beads is more than nonmagnetic ones.
- Protein adsorption and separation properties were investigated.
- The static and dynamic adsorption capacity was influenced by magnetic nanoparticles
- BSA concentration to CB density for both magnetic and nonmagnetic ones was the same

Enhancing purification efficiency of affinity functionalized composite agarose micro beads using Fe_3O_4 nanoparticles

S. Amiri, M.R. Mehrnia[1], F. Pourasgharian Roudsari

School of Chemical Engineering, College of Engineering, University of Tehran, P.O. Box 11155-4563, Tehran, Iran

Abstract

In this work, a series of magnetic and nonmagnetic agarose matrices were fabricated for protein purification. Certain amounts of Fe_3O_4 nanoparticles were encapsulated in agarose beads to form composite magnetic matrices with enhanced purification efficiency. Structure and morphology of prepared matrices were studied by optical and scanning electron microscopes, FT-IR, and BET-BJH analysis. The prepared matrices had regular spherical shape, followed by a uniform size distribution. By nanoparticles addition, the number of mesopores decreased while population of pores with radius≤10 nm increased; thus, higher specific area achieved. According to VSM results, magnetization degree was one of the characteristics affected by agarose content of the beads. A dye ligand, Cibacron Blue F3GA (CB), was covalently bound to beads to adsorb Bovine serum albumin. CB concentration was determined by elemental analysis. It was shown that magnetic beads hold higher CB concentrations than nonmagnetic ones due to higher specific area. As a result, magnetic 8%-agarose beads had the highest affinity adsorption capacity in static experiments. Moreover, breakthrough curves were monitored to calculate dynamic binding

[1] Corresponding author: Tel: (98-21) 61112184, Fax: (98-21) 6695 7784. Email: mmehrnia@ut.ac.ir

capacity. And, it was shown that magnetic 4%-agarose had the highest adsorbing amount (6.00 mg/mL). It was implied that pore diffusion in magnetic 4%-agarose may be the reason for higher dynamic capacity. Plus, column efficiency was evaluated. It was revealed that all magnetic beads had lower HETP (0.11, 0.12 and 0.11cm for magnetic 4, 6, and 8%-agarose beads) than nonmagnetic ones (P-value<0.05).

Keywords: Agarose beads; Adsorption capacity; BSA; BET-BJH analysis; Cibacrone blue F3GA; Elemental analysis; Fe_3O_4 nanoparticles; HETP; Magnetization; Spatial hindrance.

1. Introduction

Chromatography technology, with high performance efficiency, has been one of the most powerful industrial separation methods for purification of bio products in the past few decades [1-2]. Dye-ligand chromatography has played an important role in separation, purification and recovery of proteins and enzymes, since it is thrifty and stable. Plus, group specific dyes are attainable, and can be used for separation of a large number of proteins [3-7]. Nevertheless, their use is limited due to some physical properties (like compressibility) of biocompatible beads (such as agarose).

Moreover, at high flow rates, greater pressure drops occur for small beads and mass transfer is limited due to internal diffusion. Therefore, these problems should be resolved to provide higher adsorption capacity.

However, the polymer-type supports which were reported in the literature have been designed for specific purposes or are so expensive that their applications in biotechnology are quite restricted.

In addition, as a protein separation adsorbent in downstream bioprocessing, magnetic support should possess a high capacity and selectivity for protein adsorption. To achieve these goals, new methods and materials should be developed to synthesize magnetic supports for efficient protein adsorption and purification.

Polymeric hydrogels filled with magnetic nanoparticles (ferrogels) have been the subject of many studies in the past two decades. These ferrogels have been successfully developed regarding their applications in several biomedical and industrial fields [8].

The amount and size of nanoparticles in the prepared Ferrogels are varied. This cause significant difference in efficiency and physical characteristics of beads [9]. However, there has not been any specific formulation for it.

Using metal nanoparticles in agarose adsorbents exhibit considerable physical, chemical and biological properties [10]. Magnetic beads are usually made of iron oxide such as maghemite (Fe_2O_3) or magnetite (Fe_3O_4) enclosed in a nonmagnetic matrix of an inert and biocompatible material [11-12]. Iron oxide is preferred over pure iron due to better oxidative stability [9]. Recently, using magnetic bead in various applications is expanding [13-16]. Due to solving many problems associated with chromatographic separations in packed and conventional fluidized beds [17]. The main reason to use magnetic beads is their ability to be easily manipulated in a fluid flow as well as the possibility to functionalize them with a large range of biomolecules [14].

There have been several researches about magnetic particles in previous studies. They were either placed in various polymers or were coated with different polymers [8 and 18-19]

As a result, due to their different characteristics such as particle size distribution, porosity, ligand density, magnetic nanoparticle (MNP) properties and etc., that may affect adsorption, they could not be compared explicitly. However, magnetization impact on efficiency of immobilized ligands on beads has not been considered. Furthermore, the efficiency of this ligand was not compared with non-magnetic ones. But when both are made under the same conditions, the effects of nanoparticles on protein adsorption can be investigated separately.

This paper revealed that researchers can supply their required suitable beads easily. Moreover, effects of magnetization, as well as the structure of beads on protein adsorption of beads were studied. Also, BET-BJH analysis and ligand density measurement was done to investigate the effect of these nanoparticles on pore size and ligand density and therefore understand the reason for their effect on efficiency.

In this work, the prepared beads had definite amounts of magnetic particles that are distributed homogeneously throughout agarose matrix. Thus, only effect of their agarose percentage on magnetic characteristic of beads is studied. This percentage is chosen in a specific way, so to increase mechanical resistance of beads and in a way to remove beads easily by a magnet from the solution.

There upon, the properties of micro beads were analyzed. The prepared beads had high magnetization. Then, CB ligand was placed on them and their efficiency in absorbing BSA with non-magnetic beads in static and dynamic situations are studied. Moreover, dynamic adsorption capacity at 10% breakthrough (DBC 10%) was selected for discussion due to its frequent usage by other researchers [20]. Also, Column efficiency in elution step with parameters such as HETP and number of theoretical plates (N_t) is described for prepared magnetic and non-magnetic beads to study and compare them.

The obtained results were studied based on CB concentration and porosity variation of beads, in order to get more accurate conclusions.

2. Experimental

2.1. Magnetic and nonmagnetic bead preparation

Magnetic and nonmagnetic agarose beads (4, 6 and 8% wt/v agarose content) were prepared by similar reactor and apparatus to our latest work [21]. However, instead of the stirrer, a stainless steel homogenizer (5000 rpm) was used.

Fe_3O_4 nanoparticle with 30 nm average particle size, 99% purity, and 55 m^2/g specific surface area was supplied from a local producer. Different amounts of Fe_3O_4 nanoparticles (0.16, 0.32, and 0.48 g) were dispersed in agarose solution. The magnetic beads were separated with a

permanent magnet that was calibrated using the LEYBOLD DIDACTIC GMBH Tesla-meter (Hürth, Germany) according to instructions provided by manufactures.

The prepared matrices are named magnetic or nonmagnetic 4, 6, and 8%-agarose. The beads were stored at 4^{o}C in distilled water containing 0.02% (g/ml) sodium azide at pH 7.

The magnetic and nonmagnetic matrices' spherical morphology was observed by an optical microscope (BX51, Olympus).

2.2. Dye immobilization

CB was coupled to beads in the following method:

15 ml filtered beads were immersed in a 50 ml aqueous solution (2 mg dye/ml) for 30 min at 60^{o}C. This was followed by adding 3.5 g NaCl, to stimulate deposition of dye on beads. After 60 min, 12.5 g Na_2CO_3 aqueous solution (25 wt%) was added. This, by changing pH, accelerated the reaction between the dye and beads which last for 4 h at 80^{o}C. Finally, dyed beads were washed with hot water, methanol, 2 M NaCl and 0.1 M potassium phosphate aqueous solution (pH 7) successively, until no dye could be detected. Washing procedure was done in order to prevent any dye leakage during adsorption and elution. Finally, the beads were stored in 0.1 M potassium phosphate aqueous solution (pH 7) containing 0.02wt% sodium azide, at 4^{o}C. The dye content of beads was determined by Elemental Analysis (Thermo Finniger Eager 300 for EA1112).

2.3. Characterization of magnetic microspheres

2.3.1. Morphology and characteristics of the beads

For a deeper characterization, magnetic and nonmagnetic microspheres' morphology was observed by scanning electron microscope (SEM, JEOL, JSM-6700F). Before SEM imaging, beads were lyophilized (freeze-dried). Samples were frozen at -50^{o}C for 24 hours. Under vacuum (pressure 10 Pa) at -50^{o}C the beads water content removed and freeze dried particles obtained. A vibrating sample magnetometer (VSM, model-155, Digital Measurement System, Inc.) was used to measure magnetism degree of microspheres in a magnetic field. Fourier transform infrared (FT-IR) spectra (PerkinElmer Spectrum Gx,USA Perkin-Elmer company) was used to characterize magnetic and non-magnetic beads.

2.3.2. The intra-particle pore size distribution and the specific surface area of the beads

The intra-particle pore size distribution and specific surface area of the dried agarose beads, dried by freeze-drying as mentioned previously, were determined by the BET-BJH method, i.e., N_2 adsorption measurement at −196°C, with a NOVA 2000 porosimeter (Quantachrome, USA).

2.4. BSA adsorption on CB coupled magnetic and nonmagnetic microspheres

BSA was chosen as the model protein. It is found that a medium with pH 5 and a low ionic strength (0.01µS adjusting by NaCl) is more efficient in adsorbing BSA [17]. Thus, only the effect of initial protein concentration on adsorption needs to be studied to analyze affinity efficiency of functionalized magnetic beads. In a typical experiment, BSA was dissolved in 10 ml of buffer solution. Afterwards, 500 mg of magnetic/nonmagnetic microspheres (not dried) was added to protein solution. The mixtures were stirred at 100 rpm, room temperature. At specific intervals, magnetic microspheres were deposited by means of a magnet. Then, the supernatant was analyzed by spectrophotometer (at 280 nm) to determine protein concentration versus time.

2.5. Dynamic separation of BSA

Breakthrough behavior of adsorbents in a column with 1.4 mm internal diameter was investigated. In all tests the column was loaded with 2 ml of adsorbents at room temperature. After stabilizing adsorbents in the binding buffer, protein solution (1 mg/ml) was pumped into the column at 0.5 ml/min rate. The liquid flow rate was kept constant during the dynamic experiments. Effluent samples were collected in fractions (1.6 ml per fraction) from outlet of the column through the operation. Protein concentration was determined by the absorbance of effluent at 280 nm. Dynamic binding capacity (DBC), at 10% of initial concentration, was calculated from breakthrough curves which were demonstrated by Hardin et al. (2009) [22].

2.6. Dynamic desorption of protein

At this stage, BSA separation happened due to 0.5 M Thiocyanate sodium and 0.5 M NaCl in 0.5 M Tris buffer. The final BSA concentration within the desorption medium was determined spectrophotometrically at 280 nm.

2.7. Statistical analysis

The obtained data was studied by analysis of variance (ANOVA) and least significant difference (LSD) test. At least three individual examinations were performed to determine assay consistency.

3. Result and discussion

3.1. Characteristics of the beads

Fe_3O_4 nanoparticles were used in amounts of 0.16, 0.32, and 0.48 g to prepare magnetic beads in preliminary experiments (the data are not presented here). The magnetic response of the beads was evaluated by attracting them with a permanent magnet (200 mT), based on Degen et al. (2012) method. Accordingly, each time a permanent magnet was placed next to the container. Then, the separation rate caused by magnet was measured [18]. Samples containing 0.48 g nanoparticles showed faster separation rate.

Also, mechanical resistance of the matrices was investigated with pressure drop test in packed bed. It was found that the pressure drops increased linearly with increasing fluid velocity for all matrices tested. However, by increasing nanoparticle concentration to 0.48 g in gel, the rate of increasing decreased. Results showed that mechanical strength of the magnetic particles (0.48 g) was high enough for use under fluid velocities 50, 350, and 850 cm/hr for magnetic 4, 6 and 8%-agarose, respectively. This certainly benefits the demand of high productivity for affinity chromatography process.

In addition, beads' morphology and nanoparticle content remained stable during magnetic attraction. The results of former steps revealed that beads containing 0.48 g Fe_3O_4 showed maximum enhancement of mechanical resistance and attraction by magnet. Therefore, only these beads were used in the following steps.

Nonmagnetic beads (4, 6, and 8%-agarose) were characterized in our prior works [21 and 23]. Figure 1 shows optical microscopic photographs of magnetic beads. The magnetic particles are seen as fine black dots trapped within the microsphere beads. Size distributions of magnetic

beads (4, 6, and 8%-agarose) with 0.48 g of Fe_3O_4 nanoparticles are compared in Figure 2. It is seen that a large population of beads are in the range of 50-150 µm diameter.

For the next steps, both magnetic and nonmagnetic agarose beads were filtered and beads in the range of 50-150 µm were collected. This was done in order to eliminate the effects of particle size on nanoparticles and/or agarose content of the beads. Therefore, comparison of results was done with two approaches: 1- different agarose content of magnetic and nonmagnetic beads, 2- same agarose content magnetic and nonmagnetic beads.

Figure 1- Optical microscopic photographs of magnetic (a) 4%-, (b) 6%-, and (c) 8%-agarose beads

Figure 2- Particle size distributions of magnetic beads

The retention of prepared particles by the magnet indicated their magnetic behavior. In order to scientifically confirm the existence of magnetic bond and surface coating of the particles, FT-IR spectra of Fe_3O_4 nanoparticles, nonmagnetic and magnetic agarose beads were examined and demonstrated in Figure 3. For agarose beads, the wide peak at ~3450 cm^{-1} belongs to the stretching vibration of O–H groups, and the peaks at almost 2950 and 2850 cm^{-1} are assigned to the stretching vibration of C–H groups. Also, the peak around 1065cm^{-1} reveals the C–O stretching vibration from the primary alcohol in agarose [24].

In addition, it is seen that Fe_3O_4 spectrum has a peak at 590 cm^{-1} for ferrous. Same peak is observed in magnetic agarose spectrum. Therefore, presence of Fe_3O_4 nanoparticles in magnetic beads is confirmed.

Figure 3- FT-IR spectra for magnetic and nonmagnetic agarose beads, and Fe_3O_4 nanoparticles

Though the amount of consumed nanoparticles in magnetic 4%-, 6%-, and 8%-agarose beads was the same, agarose contents were different. Magnetization of functionalized beads was measured to check the effect of agarose content on magnetic characteristics of produced beads.

As described by Tong and Sun [25], iron oxide crystals with average particle size of 30 nm exhibit superparamagnetic properties. In this work, average size of utilized Fe_3O_4 nanoparticles was 30 nm. It indicates that the magnetic agarose support may be regarded as superparamagnetic. This is demonstrated by the magnetization curves which are displayed in Figure 3 using electron mass unit (EMU), showing the behavior of magnetic beads in a field with a vibrating magnetometer.

In EMU spectrum, 2000 G magnetic field was found sufficient to excite all of the dipole moments presented in 1.0 g of magnetic agarose samples. This value (2000 G) is an important designing parameter for a magnetically stabilized fluidized bed or magnetic filtration with such beads [26]. Furthermore, maximum magnetization amount for 4%, 6%, and 8%-agarose beads found to be different. Increase in beads' agarose content, decreases magnetization. One-way ANOVA with 95% confidence interval indicated that magnetization of the studied beads was significantly different for the three agarose contents (p value =0.04).

Also, the same result is reported in other works [27]. Li et al. (2011) investigated agarose covering on magnetic powder with 1% agarose for preparing beads (average size of 50-100μm).

Finally, they figured out that magnetization in aqua medium with only 1% agarose, decreased from 60 to 8.5 emu/g [24].

Figure 4- Magnetization curves of magnetic agarose beads

SEM images of lyophilized magnetic and nonmagnetic beads are shown in Figures 5 (a to f) and 6 (a to f). As seen in the figures, micro beads are spherical. It is obvious that the presence of nanoparticles changed beads' surface morphology significantly. Accordingly, it caused them to have rough surfaces.

Likewise, Degen et al. (2012) observed significant morphological changes for the prepared gels carrying 53 mg/L of magnetic hydrosol, resulting to rough surface structure with many aggregates [18].

Figure 5- Shape and structure of magnetic (a and b) 4%-, (c and d) 6%-, and (e and f) 8%-agarose beads

Figure 6- Shape and structure of nonmagnetic (a and b) 4%-, (c and d) 6%-, and (e and f) 8%-agarose beads

3.2. Ligand density

Accurate determination of ligand concentration is critical since ligand density is an important factor in determining the binding capacity and separation efficiency for affinity chromatography.

Biomimitic ligands, such as CB, exhibit increase in purification ability and specificity for targeted proteins. Thus, they provide useful tools for designing simple and effective purification protocols [28-29]. In this work, CB concentration on all beads was calculated according to nitrogen(N-) content measured by elemental analysis. The data is presented in Table 1. It is found that N-contents of magnetic beads are higher than nonmagnetic ones.

Table 1. Elemental analysis data of agarose and CB immobilized magnetic and nonmagnetic agarose beads.

Accordingly, the CB content of nonmagnetic 4, 6, and 8%-agarose beads found to be 11.53, 11.93, and 11.22 μmol/g dry bead, respectively. Also, for magnetic ones CB contents are 17.24, 17.75, and 16.84 μmol/ g dry bead for 4, 6 and 8%-agarose beads, respectively. Statistical analysis of ligand density, using two-way ANOVA with 95% confidence interval, indicated a significant difference between magnetic and nonmagnetic beads (p values of 0.00 and 0.015 for nanoparticle and agarose content, respectively).

3.3. Protein adsorption

Adsorption isotherms are commonly used for characterization of affinity adsorbents proposed for bioseparation [30-32]. The effects of initial protein concentration on adsorption capacity of CB-coupled magnetic and nonmagnetic microspheres were studied batchwise. Denizli et al. [7 and 33] and Ma et al. [17] reported that significantly low adsorption capacities were obtained in high

acidic and alkaline pH regions. Therefore, in our work the adsorption medium was adjusted at pH 5.

BSA adsorbing isotherms are represented in Figure 7. According to the isotherms, Langmuir coefficients for Eq. (1) were calculated for both magnetic and nonmagnetic beads. The results are presented in Table 2.

$$C_{ads} = \frac{C_m \times C_{eq}}{K_d + C_{eq}} \qquad \text{eq.(1)}$$

In equation 1, C_{eq} and C_{ads} are the aqueous phase protein concentration and the adsorbed protein density on beads at equilibrium, respectively. C_m is maximum adsorption capacity; and K_d *is* dissociation constant.

Also, in order to evaluate the nonspecific adsorption of BSA on unfunctionalized beads and nanoparticles, same experiments were conducted. Though virgin MNPs showed 1.38 mg BSA/ g particles adsorption, unfunctionalized magnetic beads had very negligible nonspecific adsorption~ 0.09 mg BSA/ g drained bead. Hence, it is clear that by capturing Fe_3O_4 nanoparicles inside agarose network the nonspecific affinity of nanoparticles was suppressed.

It is also found that maximum adsorption capacities of CB-coupled magnetic 4, 6, and 8%-agarose beads were 21.19, 18.02, and 32.79 mg BSA/ g drained bead, respectively. For functionalized nonmagnetic 4, 6, and 8%-agarose beads, the maximum adsorption capacities were 11.24, 10.10, and 10.77 mg BSA/ g drained bead, respectively.

Based on statistical analysis, using LSD test (95% confidence interval) between CB-coupled magnetic 6%- and 4%-agarose beads, it was found that no significant difference exists between the two samples' maximum adsorption capacity (p-value=0.30). Same results are found between

CB-coupled nonmagnetic 4%-, 6%-, and 8%-agarose beads (p-value=0.76). However, significant difference is shown between magnetic and nonmagnetic beads' maximum adsorption capacity after employing analysis of variance with 95% confidence interval (p-value<0.01).

For both magnetic and nonmagnetic samples, the experimental adsorption data was well fitted to the Langmuir equation in the defined concentration range (Table 2). Results demonstrated that all magnetic beads (4%, 6%, and 8%) had higher maximum adsorption capacities and dissociation constants compared to nonmagnetic ones (4%, 6%, 8%) (Table 2). Since the captured nanoparticles' affinity was suppressed within the agarose bead, higher maximum adsorption capacity of magnetic beads is believed to be the result of higher ligand density.

It is worthy to note that even though encapsulated Fe_3O_4 nanoparticles in agarose beads could not directly participate in BSA adsorption, their presence in the matrix enhanced BSA molecules' binding to CB ligands by changing proteins' secondary structure [34]. Based on Yang et al. (2009) there is a strong static quenching and primary electrostatic interaction between MNPs and BSA [34]. Thus, BSA conformation is influenced in the vicinity of MNPs.

Amazingly, statistical analysis of calculated ratio of adsorbed BSA on dry beads to CB density of same beads ($moles\ of\ BSA/moles\ of\ CB$) (Table 2) illustrates that neither agarose nor nanoparticles content had significant effect on the ratio (p value > 0.05). Thus, in each bead sample, equal moles of CB (4 moles on average) adsorbs 1 mole of BSA.

The increase in dissociation constant of magnetic functionalized beads could be the result of high ligand density causing spatial hindrance. Though the lower dissociation constant of nonmagnetic beads could be regarded as an advantage to avoid protein elution during the washing step, increase in K_d of magnetic beads is not too much to interfere with column recovery. The data is discussed more in section 3.5.2.

This novel observation could be studied more in depth in future for finding molecular pattern of CB taking part in adsorbing BSA. It is hypothesized that the large BSA molecule overshadows an area of the bead where several small molecules of CB are planted. Several CB molecules are either actively participating in affinity binding to several amino acids distributed on one BSA molecule or simply shaded; thus, inactivated due to spatial hindrance.

Figure 7- adsorption isotherms for prepared beads

Table 2. Equilibrium adsorption constants for prepared beads.

3.4. Pore structure and BET-BJH analysis

As mentioned previously, magnetic beads' surface roughness (SEM images), CB density, and protein adsorbtion were more than nonmagnetic ones. Thus, it was decided to use BET-BJH analysis to check if Fe_3O_4 nanoparticles are the cause of increasing available surface for ligand stabilization and protein adsorbtion.

Figure 8 indicates BJH results for pore size distribution of magnetic and nonmagnetic 6%-agarose beads. As is obvious, adding nanoparticles caused excessing the number of pores which were less than 10 nm. But, the number of mesopores decreased. This can represent the effect of shrinking pores in the presence of nanoparticles. In other words, mesopores of larger than 10 nm acted like a trap for nanoparticles. Therefore, after trapping nanoparticles, these pores were clogged and smaller pores were created. As a result, the pore size range of magnetic beads was narrowed. BJH data for pore size distribution of all other beads showed same results, hence the data is not provided here.

To summarize, nanoparticles are entrapped in large pores and caused them to change into small ones. Hypothetically, one large pore turned into two small pores. The newborn pores are larger than natural pores of agarose (which are normally 1 to 2 nm).

Figure 8- BJH pore size distribution for magnetic and nonmagnetic 6%-agarose

Total pore area (a_p) and total pore volume for magnetic and nonmagnetic 6%- and 8%-agarose beads are represented in Table 3. These two observations prove that nanoparticles caused increasing beads' porosity, but the average size of pores was declined (apparently, inner surface of pores decreased). It was figured out that shrinking pore size lead to higher porosities. Specific surface area (BET) confirms this result too.

Table 3- Total pore volume and a_p and total pore volume for magnetic and nonmagnetic 6 and 8%-agarose beads

The high value of specific area means the composite beads have abundant space to bind the functional groups for protein adsorption. Also, relatively large pore radius would benefit the passage of proteins with high molecular weight and reduce the transfer limitation [35]. In addition, Sekhavat Pour and Ghaemy (2015) observed mass transfer increase when using beads which contain nanoparticles [30]. On account of these facts, protein adsorbtion increased using magnetic agarose beads.

3.5. Column efficiency calculations in dynamic adsorption of BSA

3.5.1 Protein breakthrough behavior and dynamic binding capacity

Breakthrough experiment is a practical chromatographic approach to examine efficiency of adsorbents. Figure 9 shows breakthrough curves of BSA during binding to adsorbents in the packed bed column at the 0.5 ml/min flow.

The results revealed high DBC (at 10% breakthrough) of BSA for magnetic 4%-agarose beads as the best performance among other beads. Dynamic binding capacity of this adsorbent was 6 mg/mL, which was higher than both nonmagnetic 4%-agarose (5 mg/mL), and the magnetic beads with higher agarose content (6% and 8%-agarose) (5 mg/mL). To explain the reason, it should be noted that 4%-agarose bead is more porous than 6%- and 8%-agarose ones [36]. This higher porosity allows higher mass transfer within pores. Therewith, as mentioned previously, nanoparticle presence increased surface roughness and average pore size of magnetic 4%-agarose bead. Thus, mass transfer is improved.

This facilitation effect was also observed by other researchers in protein adsorption. For example, Liu et al (2015) figured out that magnetic nanoparticles dispersed in hydrogel have direct impact on protein penetration into hydrogel [8].

These investigations revealed that magnetic nanoparticles are effective for enhancing penetration into micro particles and micro spheres. Our observations also show same results for agarose micro beads.

Figure 9- BSA breakthrough curves at 0.5 ml/min flux.

3.5.2. Number of theoretical plates (N_t)

In the breakthrough analyzing step, feeding solution which contains protein passed over the bed until it reached saturation status. It means that proteins were not willing to be adsorbed any more. Then, binding buffer, which did not contain protein, was used to wash the column. This continued until no protein was detected in the effluent. So, the only remaining BSA proteins in bed were those which were attached to CB ligands.

In the meantime, the adsorbed BSA on beads was quite stable and not washed out during the cleaning process. It shows that high dissociation constant of magnetic beads was not too much to affect adsorption process adversely.

Afterwards, elution buffer was injected to the column. The effluent was gathered continuously. By using spectrophotometer, the protein content of every 1.6 ml effluent was measured at wavelength of 280 nm. Results are shown in Figure 10. To calculate $\mathbf{N_t}$ for a column, the following formula was used [37]:

$$N_t = 5.54\left(\frac{t_r}{W_{1/2}}\right)^2 \qquad \text{eq. (2)}$$

Where t_r is the retention time of the BSA and $W_{1/2}$ is the width of peak at half the maximum height (Figure 10).

According to eq. (2), N_t for magnetic and nonmagnetic beads was calculated and presented in Table 4. N_t for magnetic beads was higher than nonmagnetic ones. Statistical analysis asserted that this difference was significant (p-value =0.04). Higher N_t of columns packed with magnetic beads, indicated higher performance of chromatography column and better protein separation.

Figure 10- Elution as the function of matrix composition

3.5.3. Height Equivalent to the Theoretical Plate (HETP)

HETP is an index which normalizes column performance to its length. So, HETP can be used to compare performance of columns. It is defined as adsorption bed length divided by the number of theoretical plates in bed [37]:

$$HETP = \frac{lenght\ of\ column}{N_t} \qquad \text{eq.(3)}$$

The values for HETP are calculated based on eq. (3) and presented in Table 4. Since bed height was similar for all magnetic and nonmagnetic beads, it can be figured out that HETP for magnetic beads was lower.

Table 4- N_t, HETP and As for magnetic and nonmagnetic beads

3.5.4. Asymmetry (As)

Asymmetry is defined as eq.(4) [38]:

$$A_s = \frac{b}{a} \qquad \text{eq. (4)}$$

where *a* is the distance from leading edge of peak to its midpoint, and *b* is the distance from peak midpoint to the trailing edge (Figure 10). A_s is frequently measured at 10% of maximum peak height. Also values between 0.8 and 1.4 are typically suitable.

The calculated A_S amounts are represented in Table 4. It is divulged that values of A_S for all magnetic and nonmagnetic beads were in the range of 0.8 and 1.4. Therefore, column packing was suitable. Accordingly, columns' performance was not affected by loose packing of beds.

4. Conclusion

In present study, magnetic agarose microspheres were fabricated by emulsification method. They were superparamagnetic with a high magnetic saturation of 10-12 emu/g. Nanoparticle content of beads was chosen in a way to increase mechanical resistance of magnetic beads. Moreover, nanoparticle content of all three bead samples (4, 6, and 8%-agarose) was same.

The microscopic surface morphology of the magnetic matrices was observed by SEM. It is seen that magnetic nanoparticles were trapped into agarose network.

Results of VSM test showed that at low agarose content, higher magnetism was achieved. Thus, 4%-agarose bead had the maximum magnetism property (12emu/g).

An affinity dye ligand, Cibacron Blue F3GA, was chemically coupled to beads surface. CB density of beads was measured by elemental analysis. It was observed that magnetic beads had higher CB density than nonmagnetic ones. Dye ligand coupled magnetic microspheres demonstrated higher affinity adsorption capacity than nonmagnetic ones. Amongst, magnetic 8%-agarose beads had the best adsorption characteristics.

It was found out that ligand density and protein adsorbtion of magnetic beads were more than nonmagnetics. Moreover, from SEM images, it was obvious that the beads surface roughness was increased. Thus, BET-BJH analysis was employed to answer the question on nanoparticles effect on pore size and structure of beads. BJH pore size distribution results showed that adding

nanoparticles caused excessing the number of mesopores with radius <10nm, while the number of larger mesopores decreased.

Based on the results, it is concluded that magnetic nanoparticles increased surface roughness, porosity, and specific surface area of composite beads. Also, mass transfer through column was facilitated.

The protein (BSA) adsorption isotherms were determined based on bachwise experiments. They followed Langmuir model. Comparison of magnetic and nonmagnetic beads containing same agarose content revealed that magnetic ones had higher static and dynamic absorption capacities. However, in static adsorption, magnetic 8%-agarose beads performed more satisfactorily, while magnetic 4%-agarose beads had the best dynamic performance. This might be due to higher porosity of 4% -agarose beads which accelerates mass transfer rate in dynamic status.

Also, calculated N_t for magnetic beads confirmed that they perform better in chromatography column rather than nonmagnetic ones. These characteristics prove that affinity functionalized magnetic microspheres are promising tools for separation and purification of proteins.

References

[1] J. Zhao, S. Yao, D. Lin, Adsorbents for Expanded Bed Adsorption: Preparation and Functionalization Chin. J. Chem. Eng., 17, (2009), 678-687.

[2] M. Ebrahimpour, M.H. Shahavi, M. Jahanshahi, G. Najafpour, anotechnology in Process Biotechnology: Recovery and Purification of Nanoparticulate Bioproducts Using Expanded Bed Adsorption. , Dynam. Biochem. Process Biotechnol. Mol. Biol., 3 (2), (2009), 57-60.

[3] F. Quadri, P.D.G. Dean, The use of various immobilized triazine affinity dyes for the purification of 6-phosphogluconate dehydrogenase from Bacillus Stearothermophilus, Biochem. J. 191 (1980), 53-62.

[4] C.R. Lowe, M. Hans, N. Spibey, W.T. Drabble, The purification of inosine 50-monophosphate dehydrogenase from Escherichia Coli by affinity chromatography on immobilized Procion dye, Anal. Biochem. 104 (1980), 23-28.

[5] C.R. Lowe, D.A.P. Small, A. Atkinson, Some preparative and analytical applications of triazine dyes, Int. J. Biochem. 13, (1981), 33-40.

[6] P.D.G. Dean, D.H. Watson, Protein purification using immobilized triazine dyes, J. Chromatogr., 165, (1979), 301-319.

[7] A. Denizli, A. Tuncel, A. Kozluca, K. Ecevit, E. Piskin, Cibacron Blue F3G-A attached poly(vinyl alcohol) particles for albumin adsorption, Sep. Sci. Technol., 32, (1997), 103-113.

[8] T.-Y. Liu, T.-Y. Chan, K.-S. Wang and H.-Mi. Tsou, Influence of magnetic nanoparticle arrangement in ferrogels for tunable biomolecule diffusion, RSC Adv., 2015, 5, 90098.

[9] G.L. Rorrer, T.y. Hsien, J.D. Way, Synthesis of porous magnetic chitosan beads for removal of cadmium ions from waste waters, Ind. Eng.Chem.Res. 1993, 32, 2170-2178.

[10] B. Domènech, M. Muñoz, D. Muraviev, J. Macanás, Polymer-Silver Nanocomposites as Antibacterial materials. Microbial pathogens and strategies for combating them: science, technology and education. Formatex, 2013, Badajoz. ISBN (13) Volume 1: 978-84-939843-9-7. Méndez-Vilas A. ed

[11] M. A. M. Gijs, Magnetic bead handling on-chip: new opportunities for analytical applications, Microfluid. Nanofluidics, 1, (2004), 22-40.

[12] R. M. Cornell and U. Schwertmann, The Iron Oxides: Structure Properties, Reactions, Occurrence and Uses. VCH, Weinheim, Germany, 2003.

[13] O. Philippova, A. Barabanova , V. Molchanov , A. Khokhlov , Magnetic polymer beads: Recent trends and developments in synthetic design and applications, European Polym. J., 47 (2011), 542–559.

[14] Y. Moser, T. Lehnert and M. A. M. Gijs, Quadrupolar magnetic actuation of superparamagnetic particles for enhanced microfluidic perfusion, Appl. Phys. Lett. 94 (2), (2009), *022505*.

[15] I. Safarik, M. Safarikova, Magnetic techniques for the isolation and purification of proteins and peptides, Biomagn. Res. Technol., 2, (2004), 7-15.

[16] Z.-Y. Ma, Y.-P. Guan, H.-Z. Liu Affnity adsorption of albumin on Cibacron Blue F3GA-coupled non-porous micrometer-sized magnetic polymer microspheres, Reactive & Functional Polym., 66, (2006), 618–624.

[17] B. Xue, Y. Sun, Protein adsorption equilibria and kinetics to a poly(vinyl alcohol)-based magnetic affinity support, J. Chromatogr. A., 921, (2001), 109-119.

[18] P. Degen, S. Leick, F. Siedenbiedel, H. Rehage, Magnetic switchable alginate beads, Colloid Polym Sci, 290, (2012), 97–106.

[19] X.-D. Tong, Y. Sun, Agar-Based Magnetic Affinity Support for Protein Adsorption, Biotechnol. Prog., 2001, 17, 738-743.

[20] R. Ghosh, T. Wong, Effect of module design on the efficiency of membrane chromatographic separation processes, J. Membr. Sci., 281, (2006), 532–540.

[21] S.Amiri, M.R. Mehrnia, Preparation and characterization of controlled sized agarose beads by emulsification technique, IChEC 2015, Iran, Shiraz

[22] A.M. Hardin, C. Harinarayan, G. Malmquist, A. Axen, R. van Reis, Ion exchange chromatography of monoclonal antibodies: Effect of resin ligand density on dynamic binding capacity, J. Chromatogr. A 1216, (2009), 4366–4371.

[23] S.Amiri, M.R. Mehrnia, Effect of controlled particle size on pore size distribution and mechanical resistance of agarose beads for chromatography application, submitted to Powder Tec. Initial Date Submitted: Mar 12, 2016.

[24] J. Li, Z. Guo, S. Zhang, X. Wang, Enrich and seal radionuclides in magnetic agarose microspheres, Chem. Eng. J., 172, (2011), 892– 897.

[25] X. D. Tong and Y. Sun, Application of Magnetic Agarose Support in Liquid Magnetically Stabilized Fluidized Bed for Protein Adsorption, Biotechnol. Prog., 19, (2003), 1721-1727.

[26] E. B. Altıntaş, A. Denizli, Monosize magnetic hydrophobic beads for lysozyme purification under magnetic field, Materials Sci. Eng. C, 29, (2009), 1627–1634.

[27] J.Y. Huang, L. Bao, X. Mao, S.Q. Tang, Synthesis of agarose –graft-hyaluronan copolymer and its potential application as a peptide carrier, J. Appl. Polymer Sci., 117, 3568-3574 (2010)

[28] N.E. Labrou, A. Karagouni and Y.D. Clonis (1995), Biomimetic dye affinity adsorbents for enzyme purification Application to one step purification of candida boidinii formate dehydrogenase, Biotechnol. Bioeng. 48, 278-288.

[29] S. Melissis, D. Rigdeu, Y.D. Clonis (2001) A new family of biomimetic ligands for affinity chromatography of glutathione-recognising enzymes. J. Chromatogr.A, 917 29-42.

[30] Z. Sekhavat Pour, M. Ghaemy, Removal of dyes and heavy metal ions from water by magnetic hydrogel beads based on poly(vinyl alcohol)/carboxymetyl starch-g-poly(vinyl imidazole), RSC Advances, 79 (5), (2015) , 64106-64118.

[31] K. Vijayaraghavan, T.V.N. Padmesh, K. Palanivelu, M. Velan, Biosorption of nickel(II) ions onto Sargassum wightii: application of two-parameter and three parameter isotherm models, J. Hazard. Mater., B133, (2006) ,304– 308.

[32] K.Y. Foo, B.H. Hameed, Review: Insights into the modeling of adsorption isotherm systems, Chem. Eng. J., 156, (2010), 2–10.

[33] A. Denizli, G. Kokturk, H. Yavuz, E. Piskin, Dye-ligand column chromatography: Albumin adsorption from aqueous media and human plasma with dye-affinity microbeads, J. Appl. Polym. Sci., 74, (1999), 2803-2810.

[34] Q. Yang, J. Liang, and H. Han, Probing the Interaction of Magnetic Iron Oxide Nanoparticles with Bovine Serum Albumin by Spectroscopic Techniques, J. Phys. Chem. B, 113, (2009), 10454–10458.

[35] Z.J. Miao, D.Q. Lin and S. J. Yao (2005) Preparation and characterization of cellulose stainless steel powder composite particles for expanded bed application. Ind.Eng. Chem. Res. 44, 8218-8224.

[36] N. Pernodet, M. Maaloum, B. Tinland, Pore size of agarose gels by atomic force microscopy, Electrophoresis , 18(1), (1997) , 55–58

[37] K. H. Row, C. H. Lee, Correlation of HETP and experimental variables in preparative liquid chromatography, Korean J. Chem. Eng.,16(1), (1999), 22-27.

[38] S. C. Siu, C. Chia, Y. Mok, P. Pattanaik, Packing of large-scale chromatography columns with irregularly shaped glass based resins using a stop-flow method, Biotechnology Progress, 30 (6), (2014), 1319–1325.

Table 1-Elemental analysis data of agarose and CB immobilized magnetic and nonmagnetic agarose beads.

Sample	C(%)	H(%)	N(%)
Simple agarose [27]	41.930	7.000	-0.420
CB immobilized 4%-agarose	36.060	5.121	0.113
CB immobilized Magnetic 4%-agarose	36.107	5.300	0.169
CB immobilized 6%-agarose	36.360	5.257	0.117
CB immobilized Magnetic 6%-agarose	36.878	5.734	0.174
CB immobilized 8%-agarose	37.087	6.000	0.110
CB immobilized Magnetic 8%-agarose	40.767	6.718	0.165

Table 2- Equilibrium adsorption constants for prepared beads.

	K_d (mg BSA/g beads)	C_m (mg BSA/g drained beads)	max BSA concentration (mol BSA/g dry beads)	ratio of max BSA concentration (mol BSA) to ligand density	the correlation coefficient R^2
nonmagnetic 8%-agarose	0.89±0.05	10.77±0.11	2.49±0.12	4.50±0.22	0.963
magnetic 8%-agarose	8.99±0.06	32.79±0.49	5.34±0.27	3.17±0.16	0.993
nonmagnetic 6%-agarose	1.10±0.06	10.10±0.25	2.92±0.15	3.46±0.17	0.920
magnetic 6%-agarose	3.09±0.03	18.02±0.20	4.04±0.20	4.39±0.29	0.957
nonmagnetic 4%-agarose	1.07±0.04	11.24±0.10	4.12±0.20	2.73±0.13	0.937
magnetic 4%-agarose	6.71±0.10	21.19±0.39	5.69±0.28	3.03±0.15	0.968

Table 3- Total pore volume and a_p and total pore volume for magnetic and nonmagnetic 4 6 and8%-agarose beads.

Sample	a_p (m^2/g)	total pore volume(cm^3/g)
CB immobilized nonmagnetic 6%-agarose	1.1591	$1.71*10^{-3}$
CB immobilized Magnetic 6%-agarose	0.0063	$81.36*10^{-3}$
CB immobilized nonmagnetic 8%-agarose	2.5925	$4.09*10^{-3}$
CB immobilized Magnetic 8%-agarose	0.0312	$43.56*10^{-3}$

Table 4- N_t , HETP and A_s for magnetic and non-magnetic beads

	N_t	HETP (cm)	A_s
nonmagnetic 8%-agarose	9.08	0.13	0.87
magnetic 8%-agarose	10.72	0.11	0.80
nonmagnetic 6%-agarose	9.85	0.12	0.92
magnetic 6%-agarose	10.85	0.11	0.87
nonmagnetic 4%-agarose	9.85	0.12	1.00
magnetic 4%-agarose	10.67	0.11	1.25

Figure captions

Figure 11- Optical microscopic photographs of magnetic (a) 4%, (b) 6%, and (c) 8%-agarose beads

Figure 12- Particle size distributions of magnetic beads

Figure 13- FT-IR spectra for magnetic and nonmagnetic agarose beads, and Fe_3O_4 nanoparticles

Figure 14- Magnetization curves of magnetic agarose beads

Figure 15- Shape and structure of magnetic (a and b) 4%-, (c and d) 6%-, and (e and f) 8%-agarose beads

Figure 16- Shape and structure of nonmagnetic (a and b) 4%-, (c and d) 6%-, and (e and f) 8%-agarose beads

Figure 17- adsorption isotherms for prepared beads

Figure 18- BJH pore size distribution for magnetic and nonmagnetic 6%-agarose

Figure 19- BSA breakthrough curves at 0.5 ml/min flux.

Figure 20- Elution as the function of matrix composition

Figure 1 a

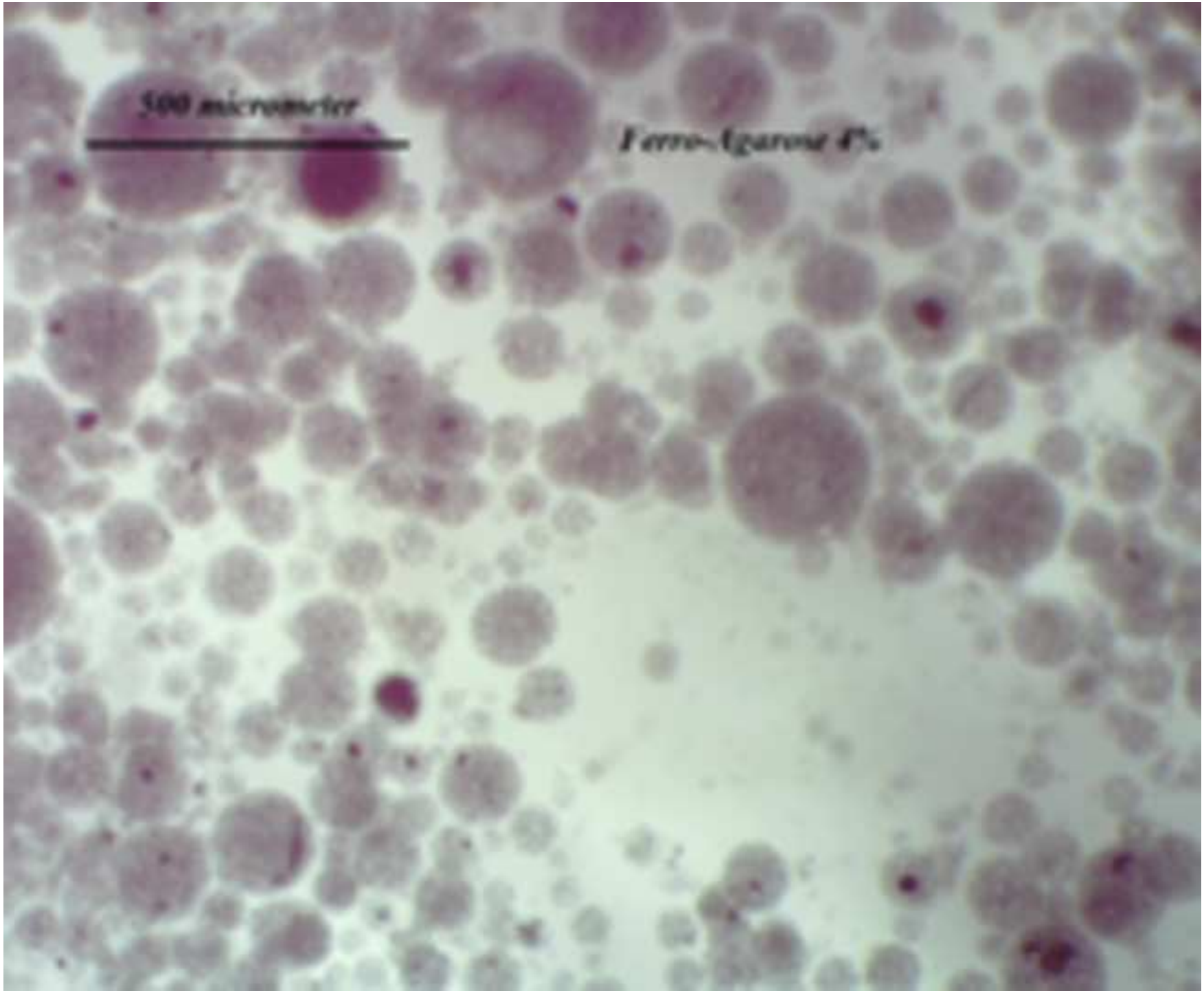

Figure 1 b

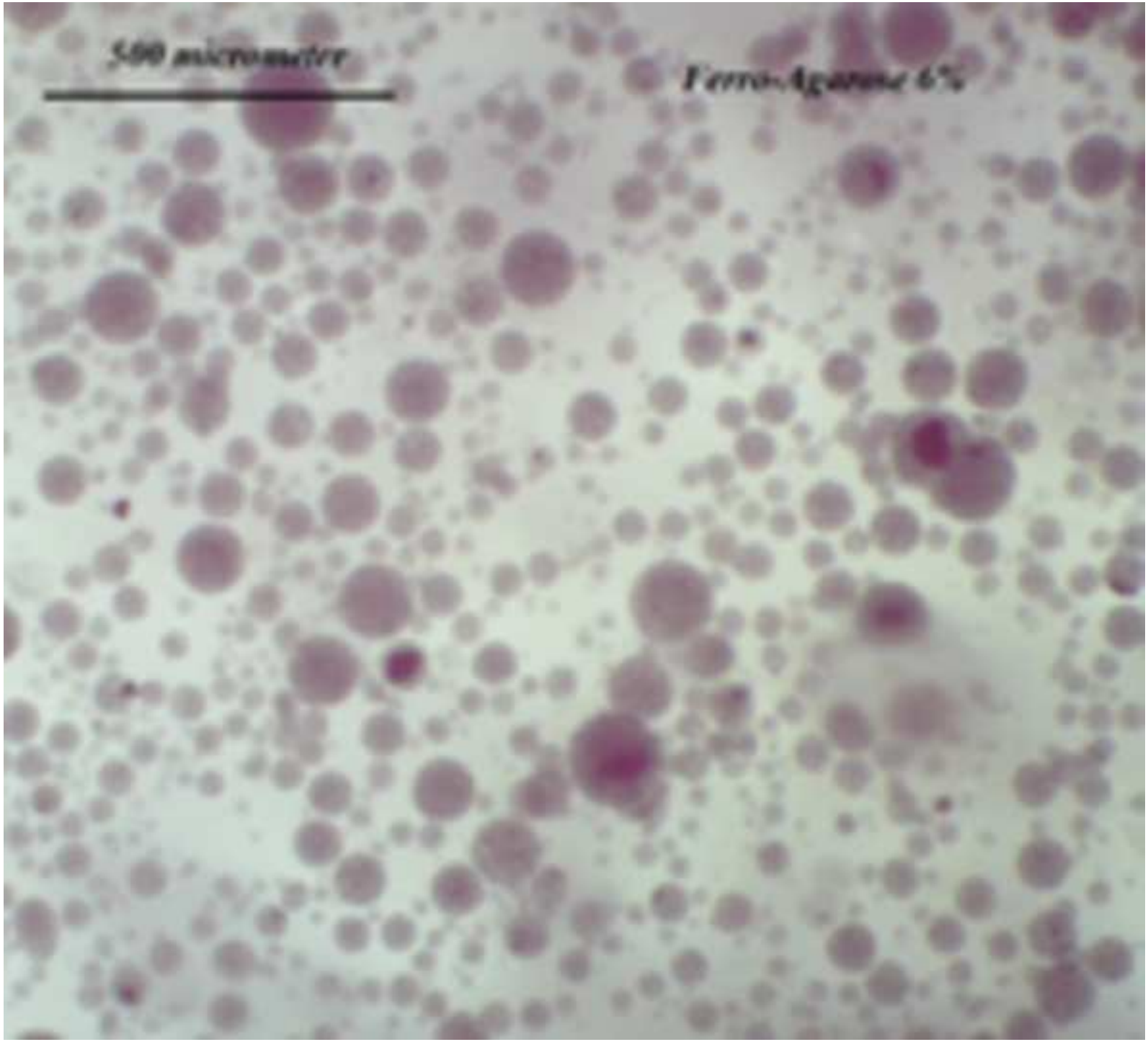

Figure 1 c

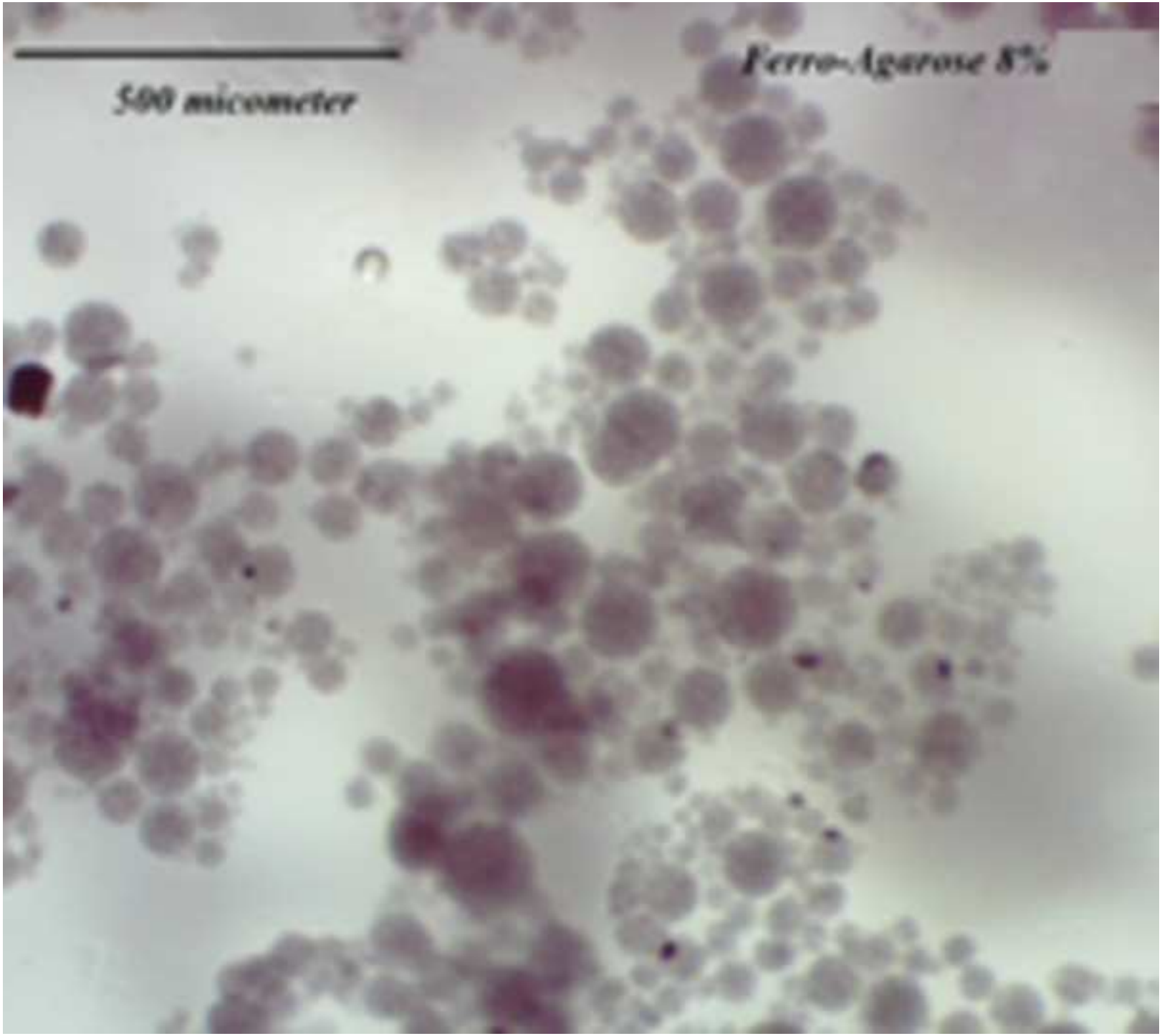

Figure 2 revised

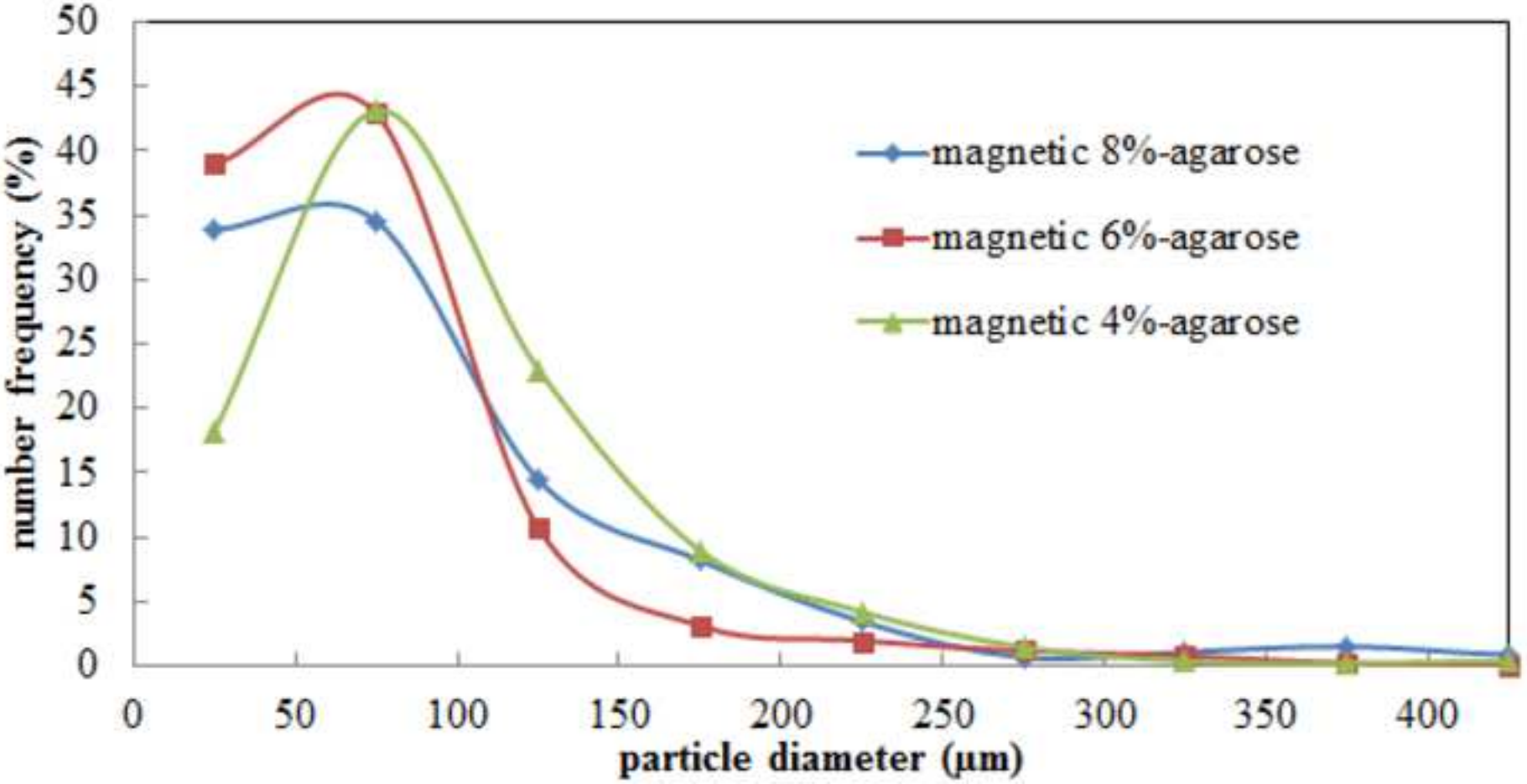

Figure 3

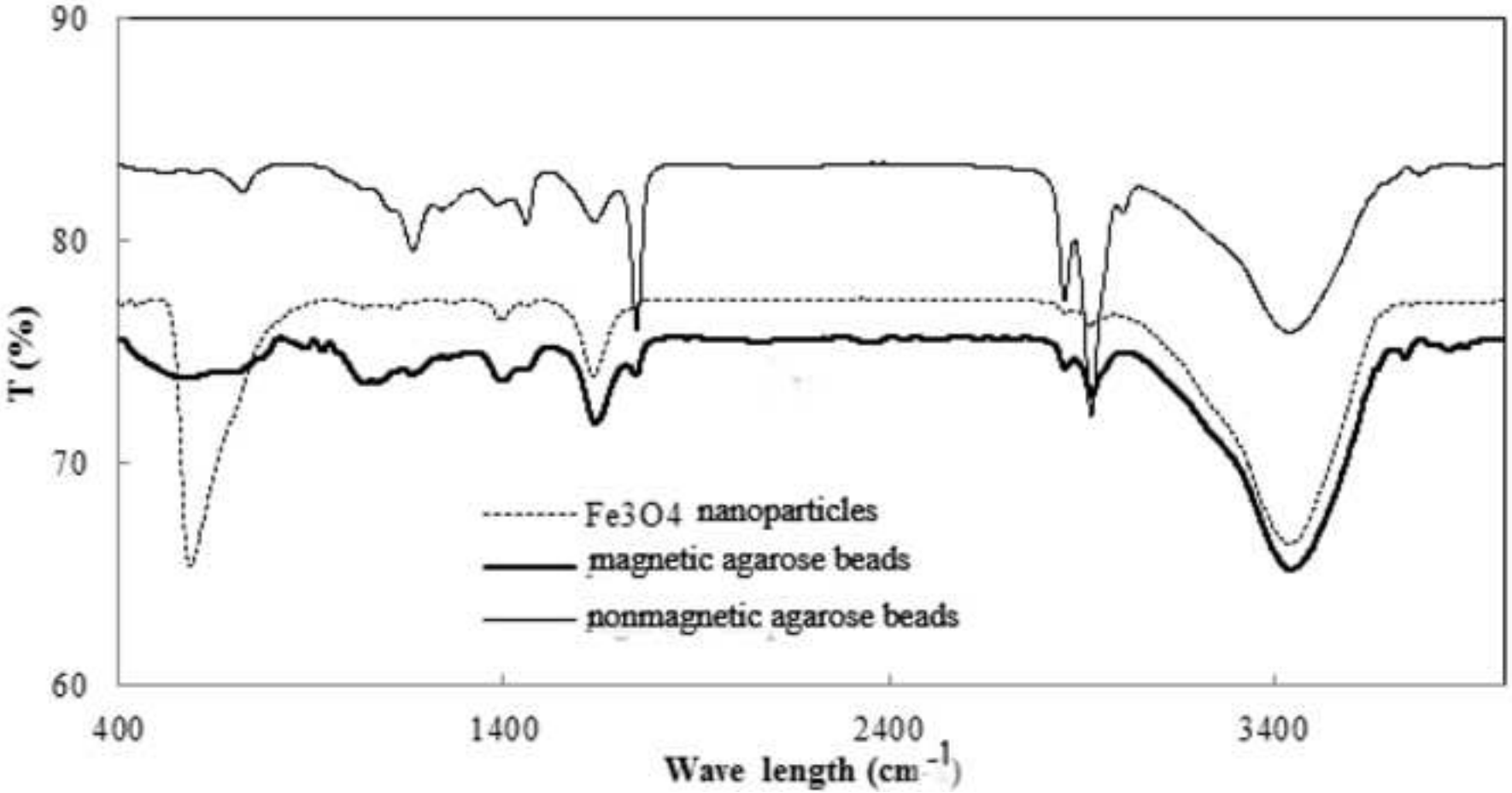
90
80
70
60
T (%)
400
1400
2400
3400
Wave length (cm-1)
Fe3O4 nanoparticles
magnetic agarose beads
nonmagnetic agarose beads

Figure 4

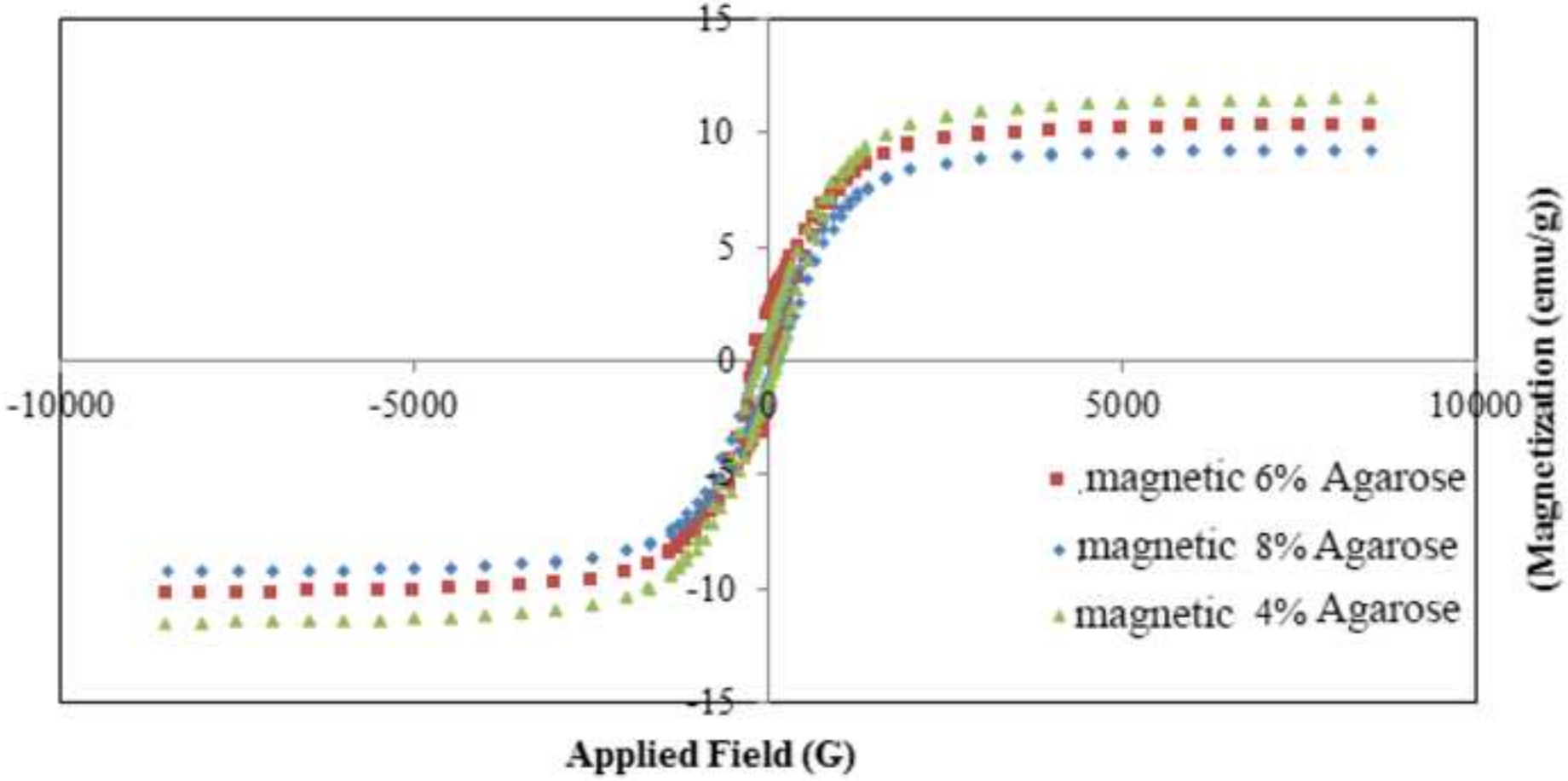
15
10
5
0
-5
-10
-15
-10000
-5000
0
5000
10000
magnetic 6% Agarose
magnetic 8% Agarose
magnetic 4% Agarose
(Magnetization (emu/g))
Applied Field (G)

Figure 5 a

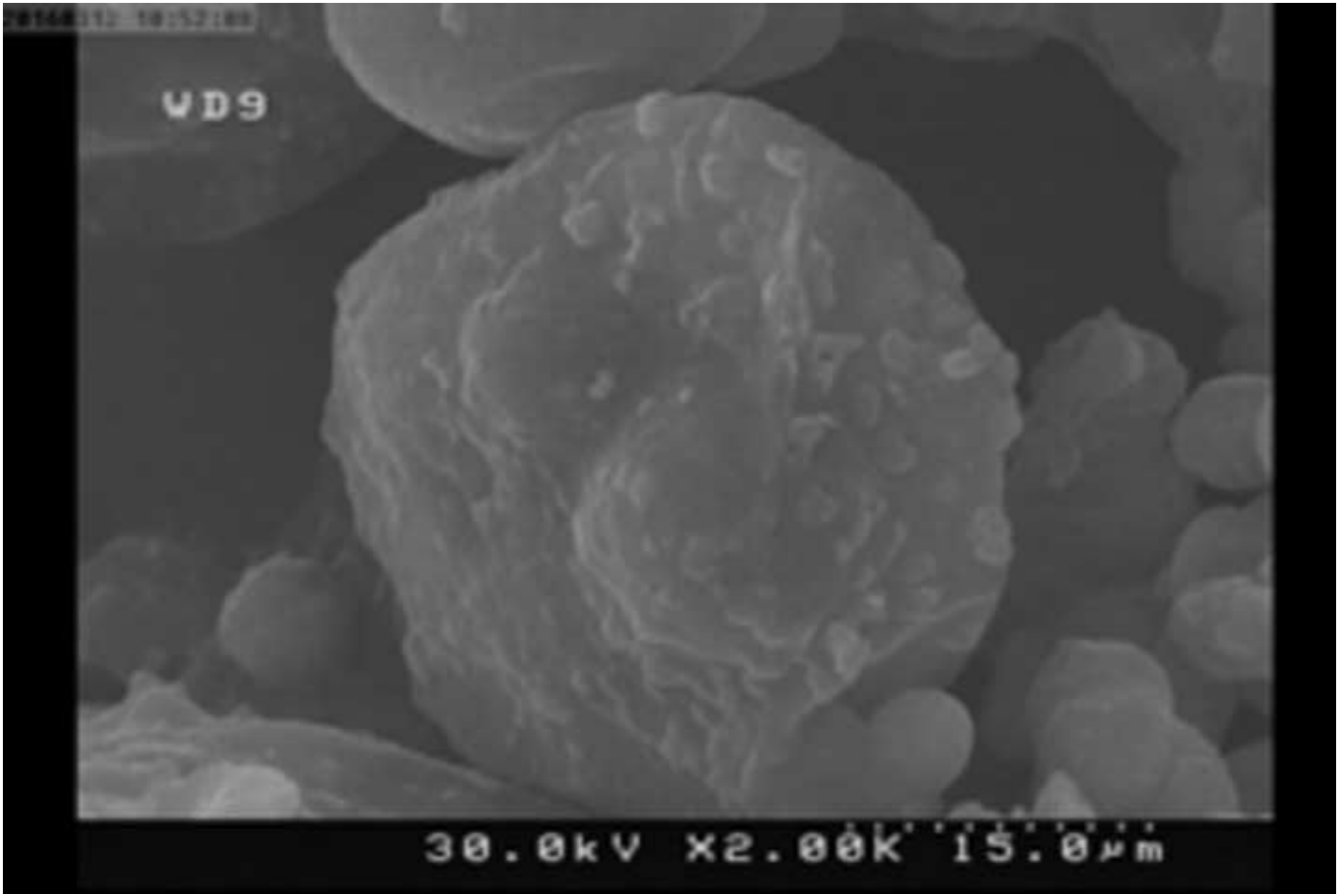

Figure 5 b

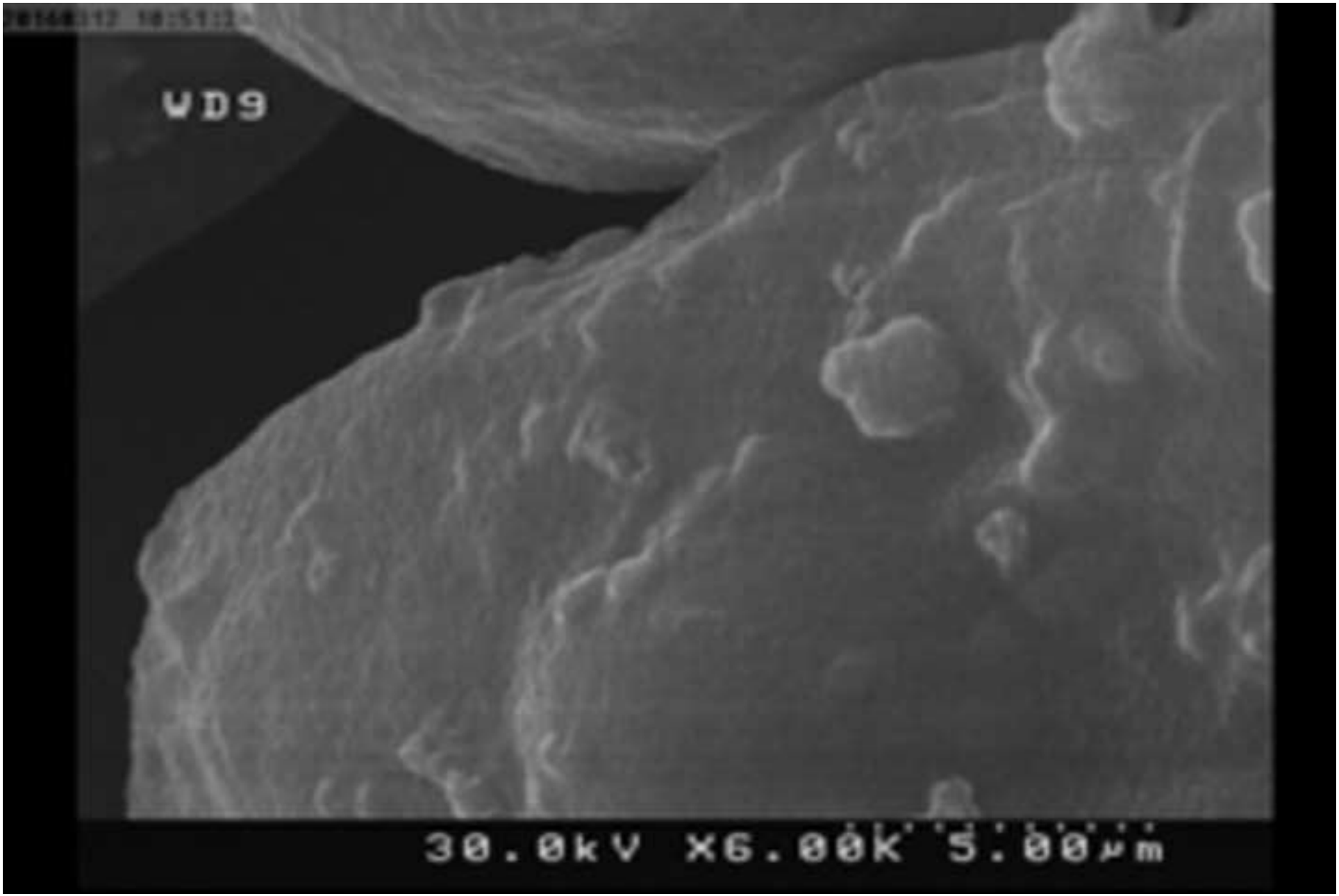

Figure 5 c

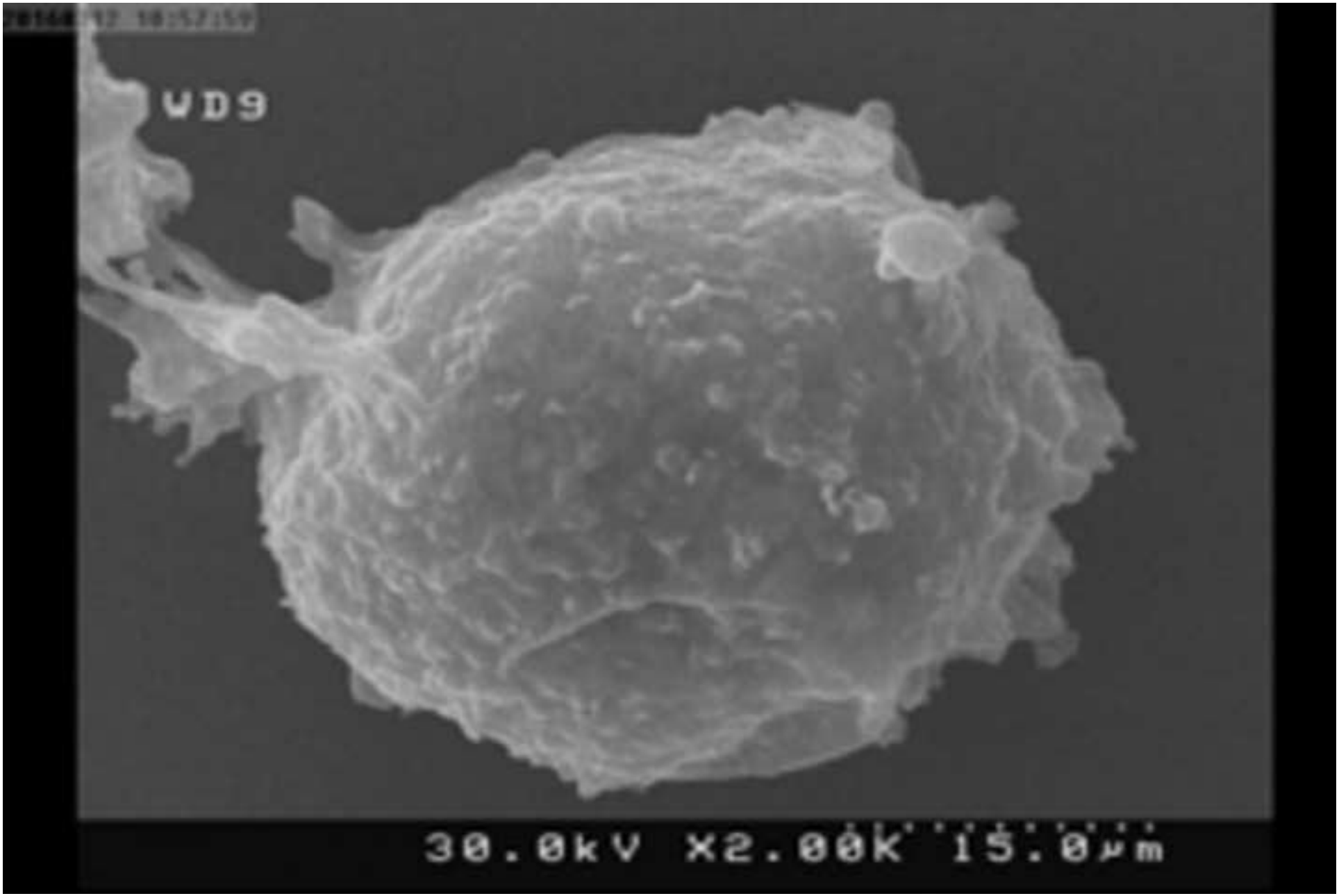

Figure 5 d

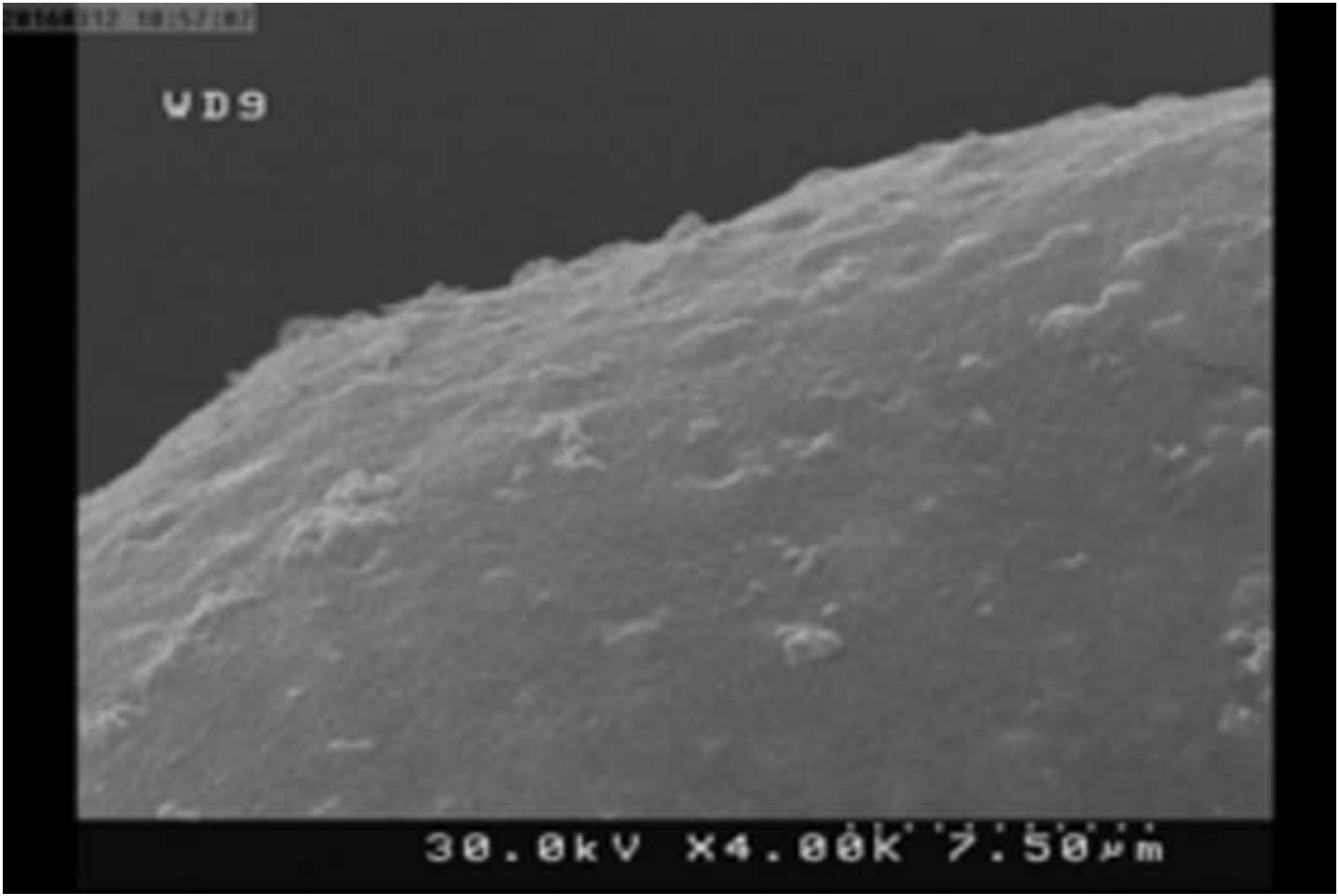

Figure 5 e

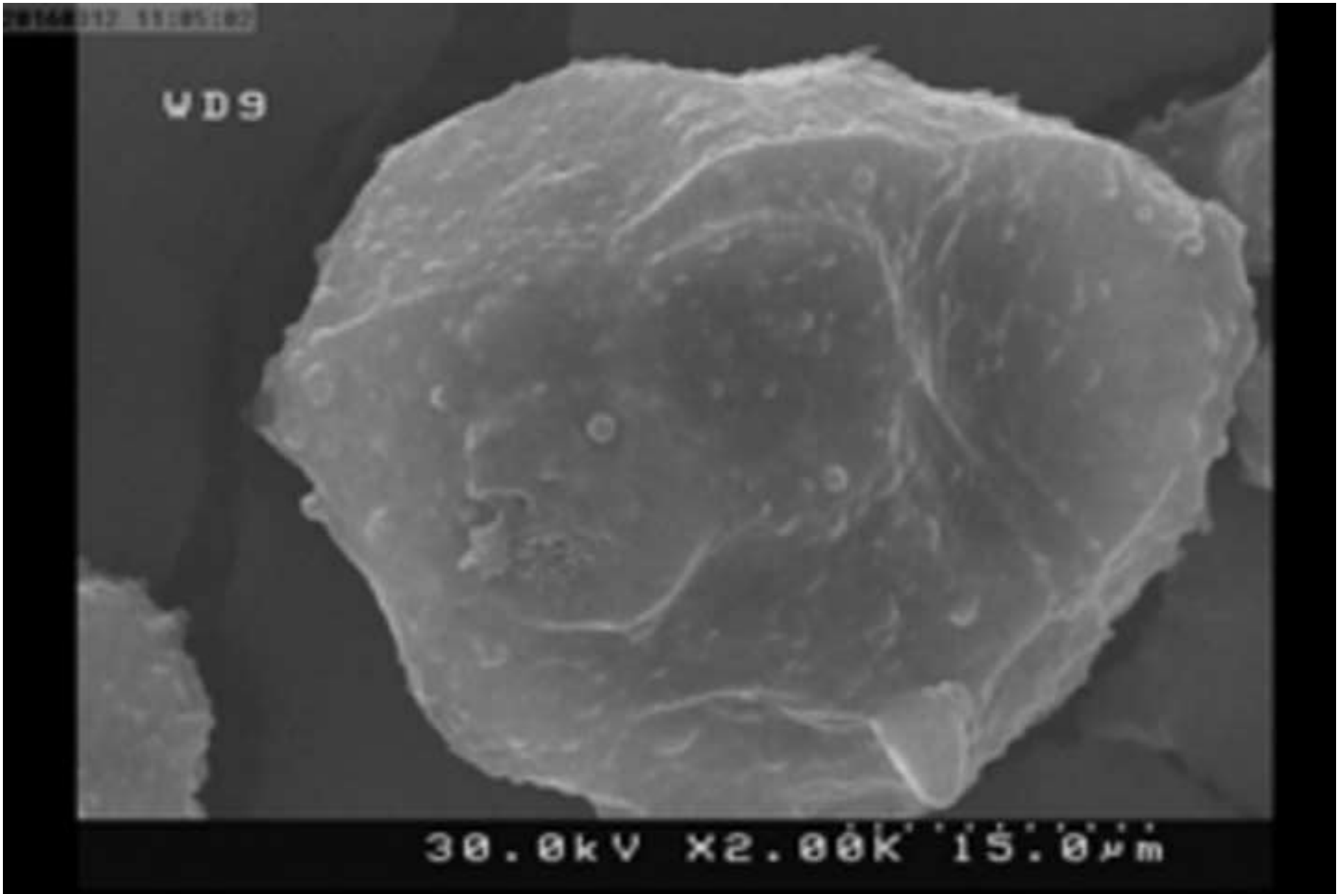

Figure 5 f

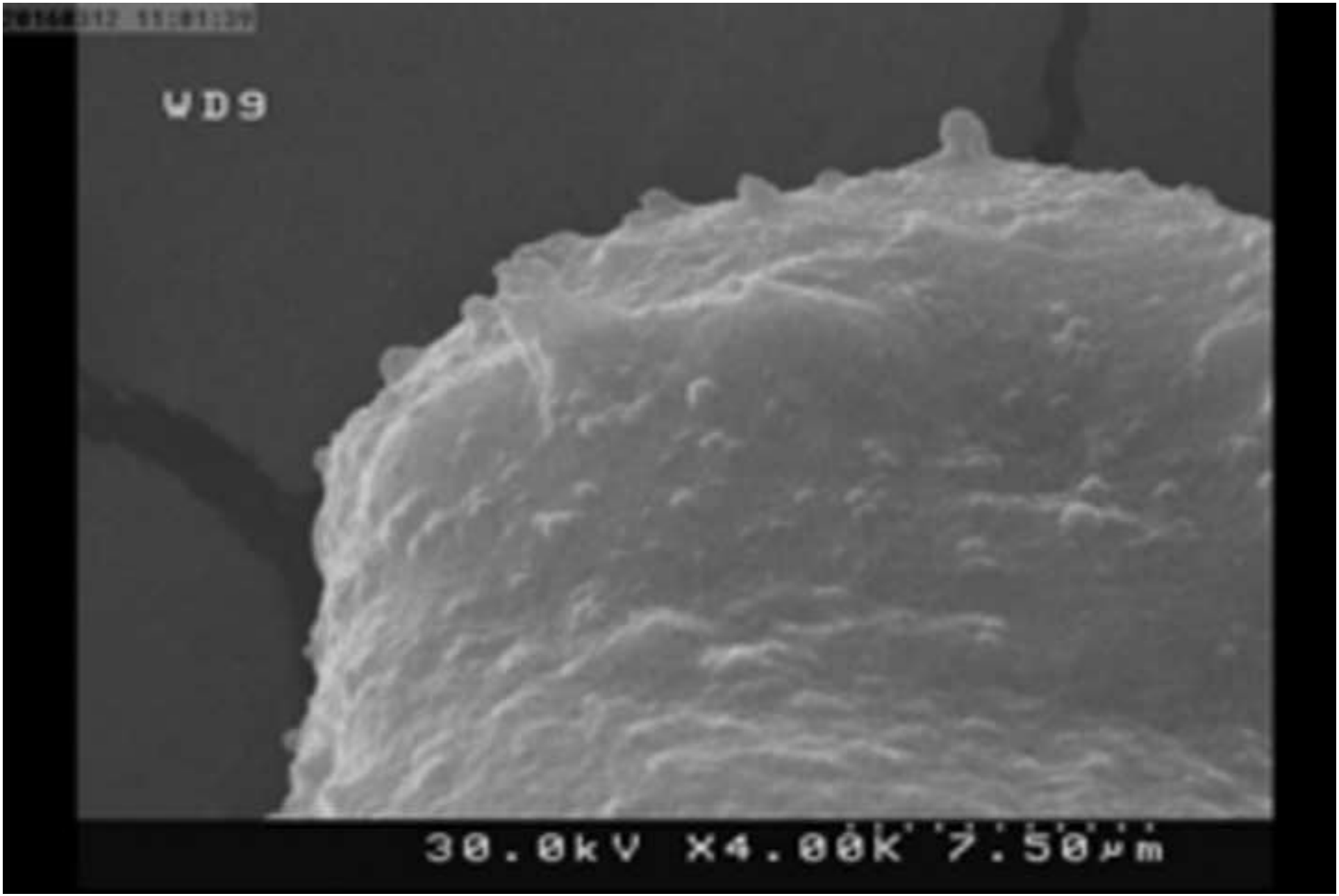

Figure 6 a

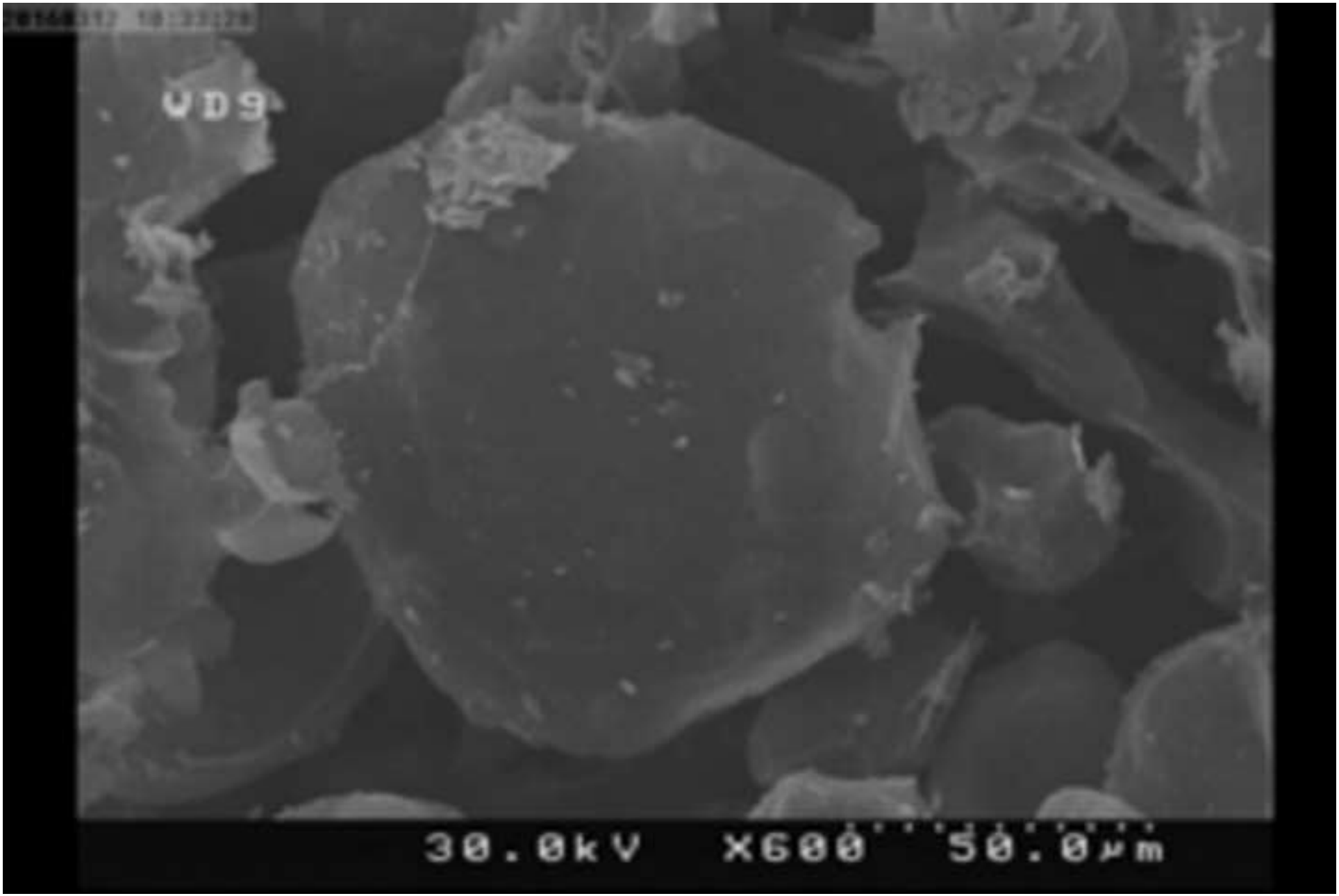

Figure 6 b

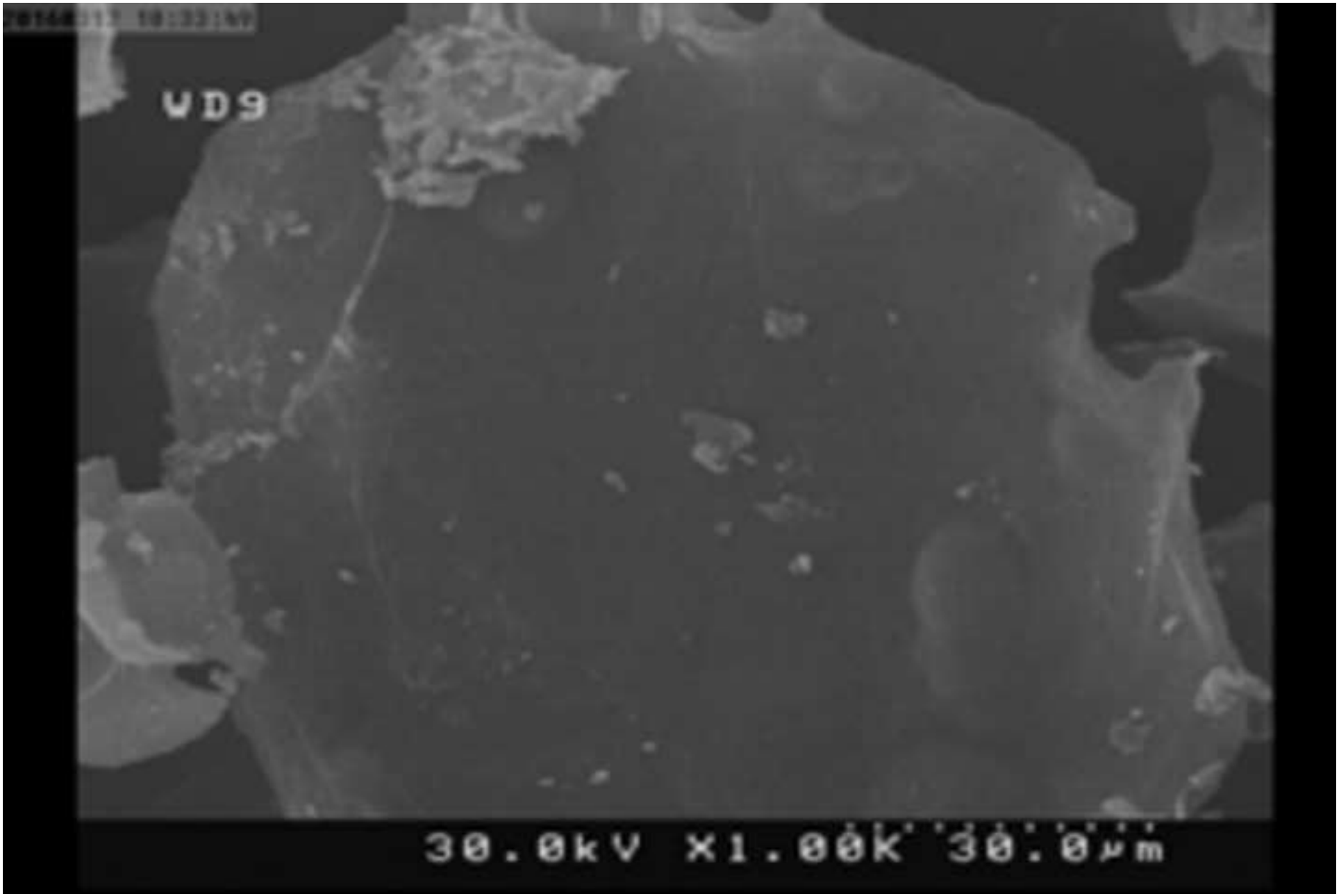

Figure 6 c

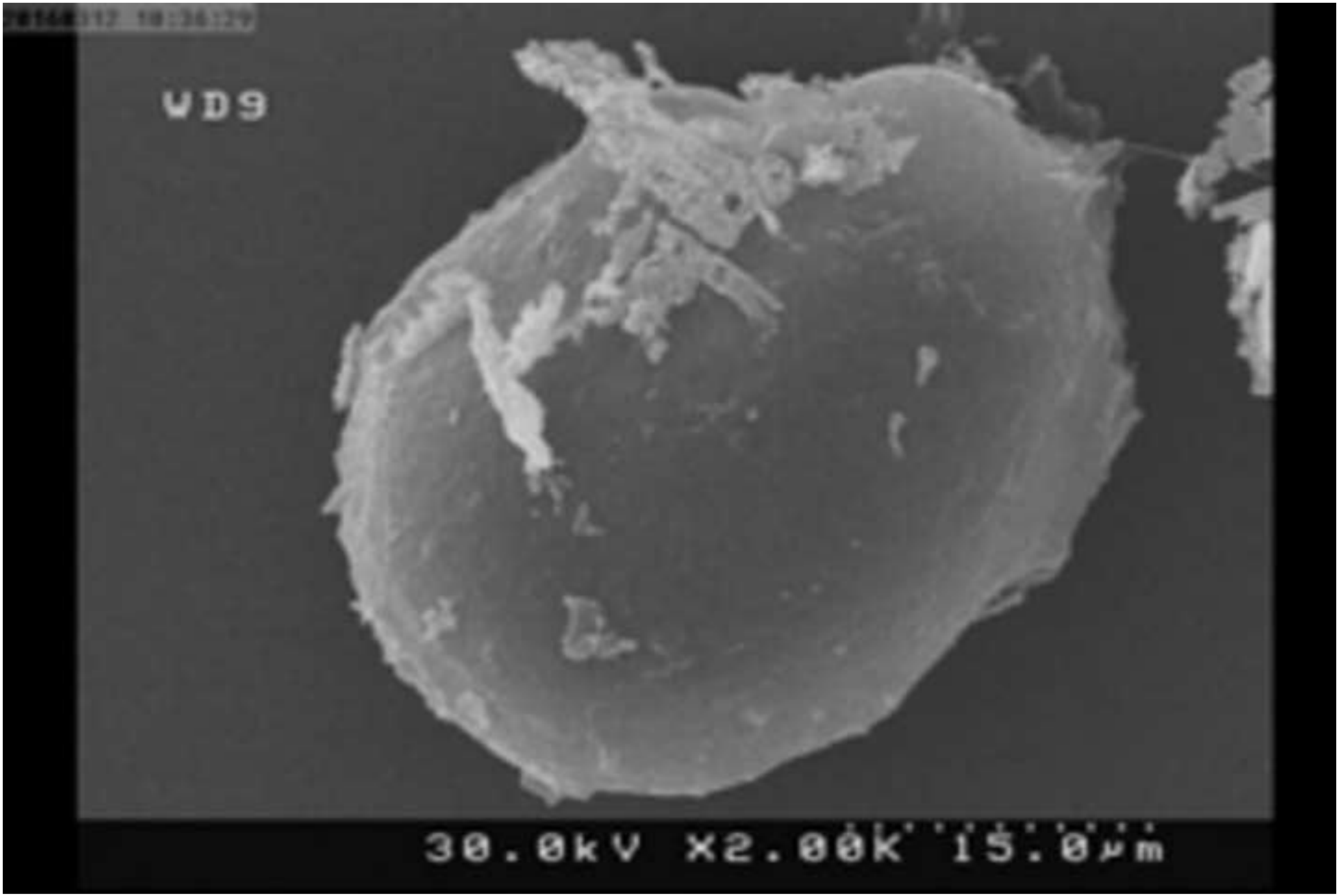

Figure 6 d

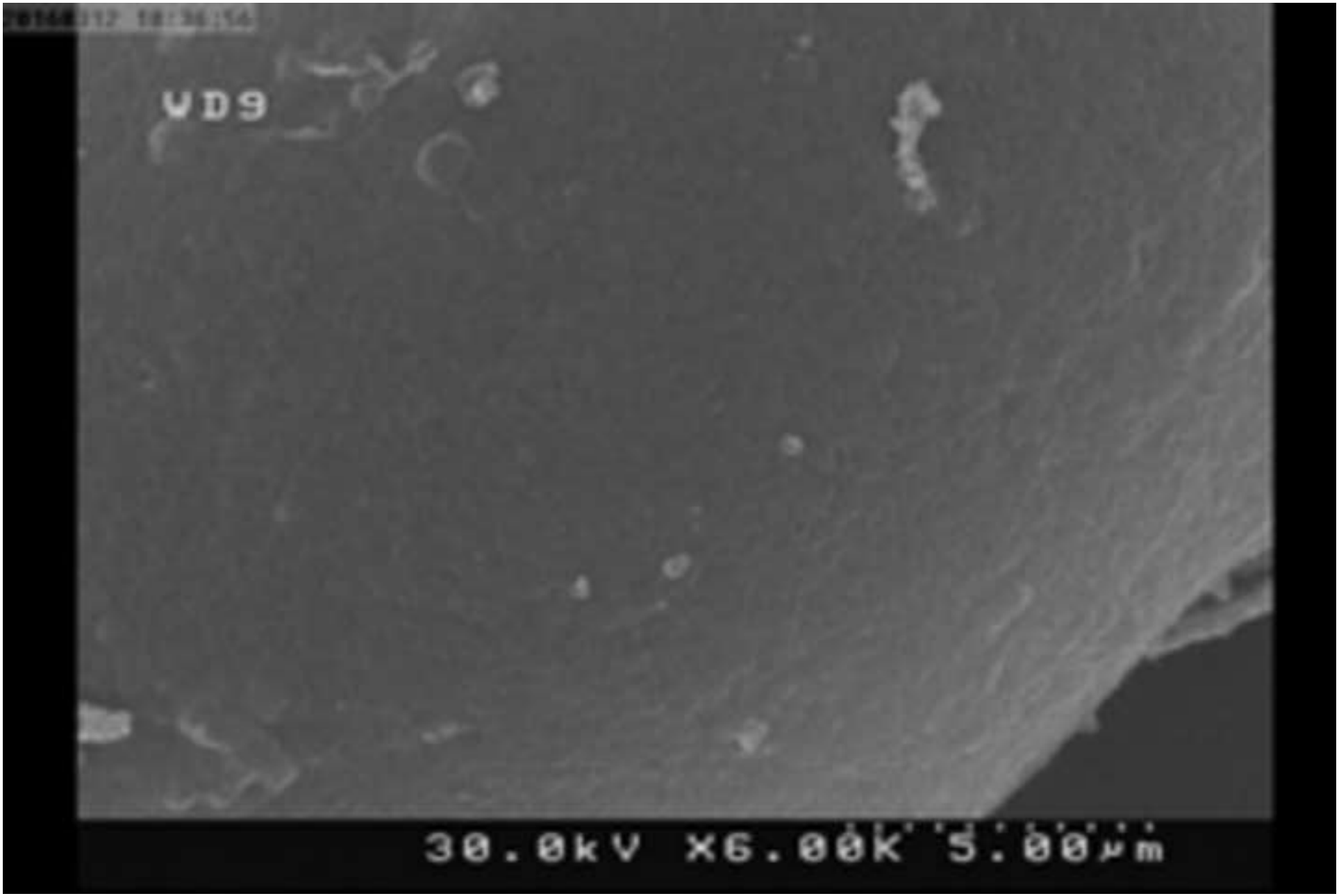

Figure 6 e

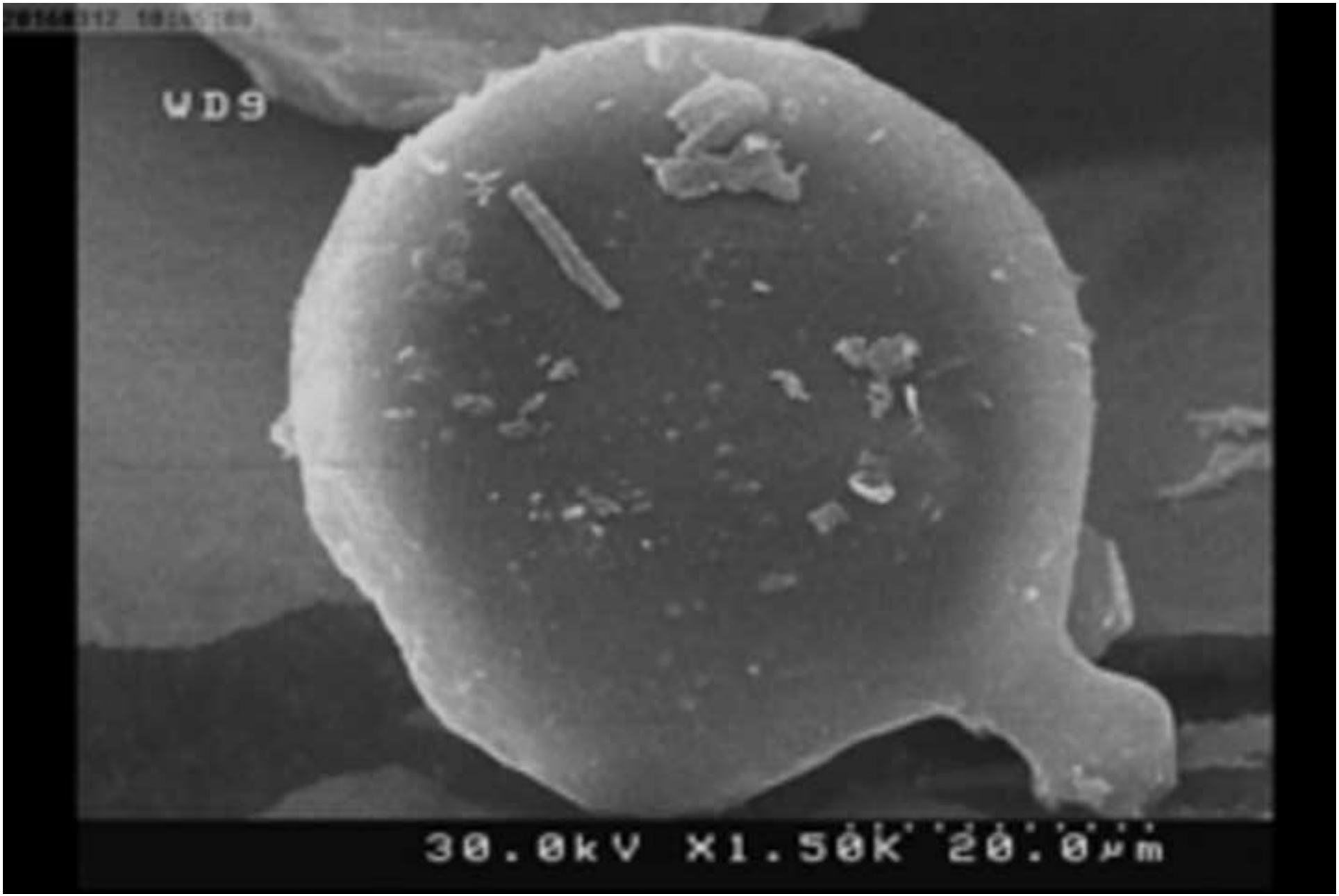

Figure 6 f

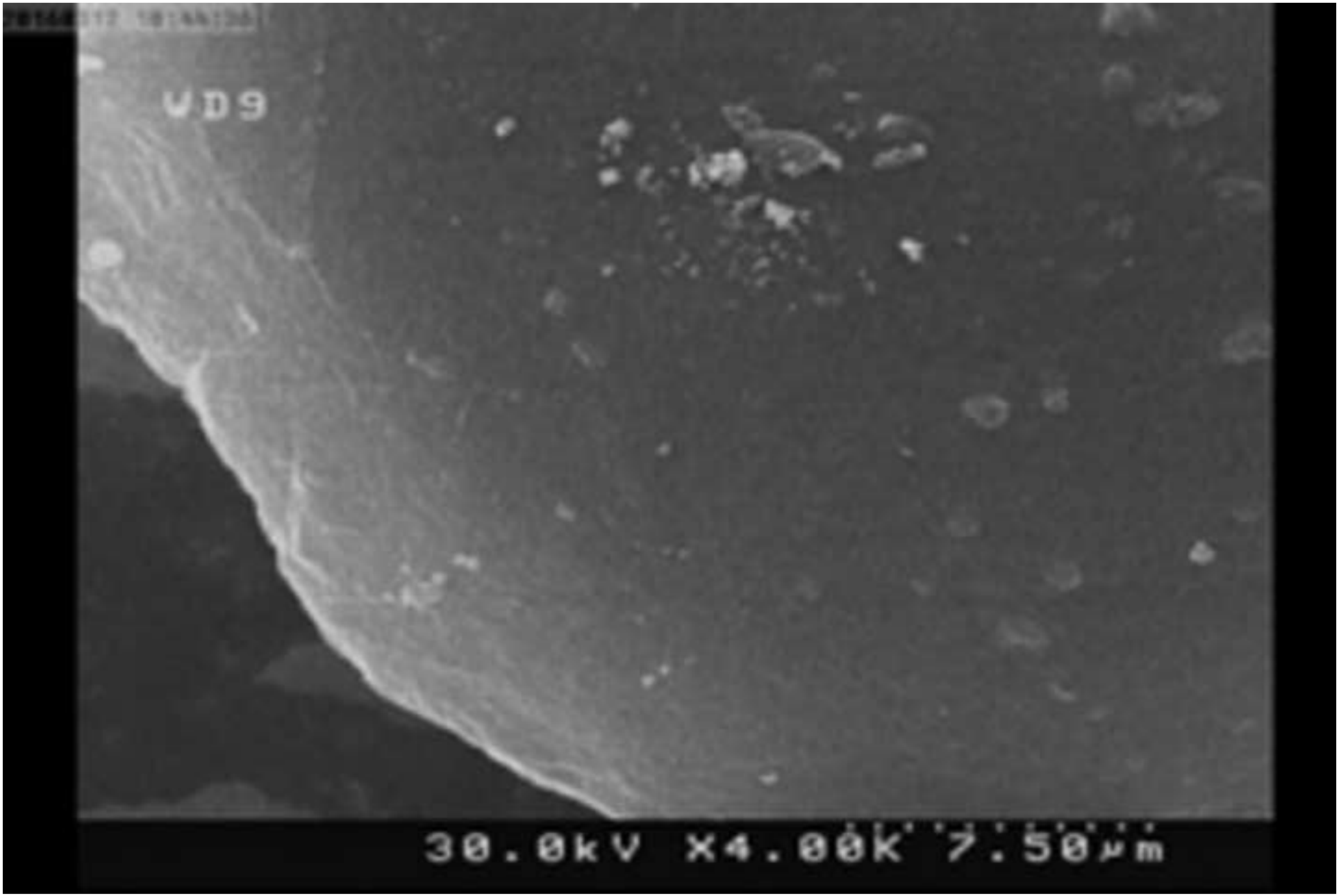

Figure 7

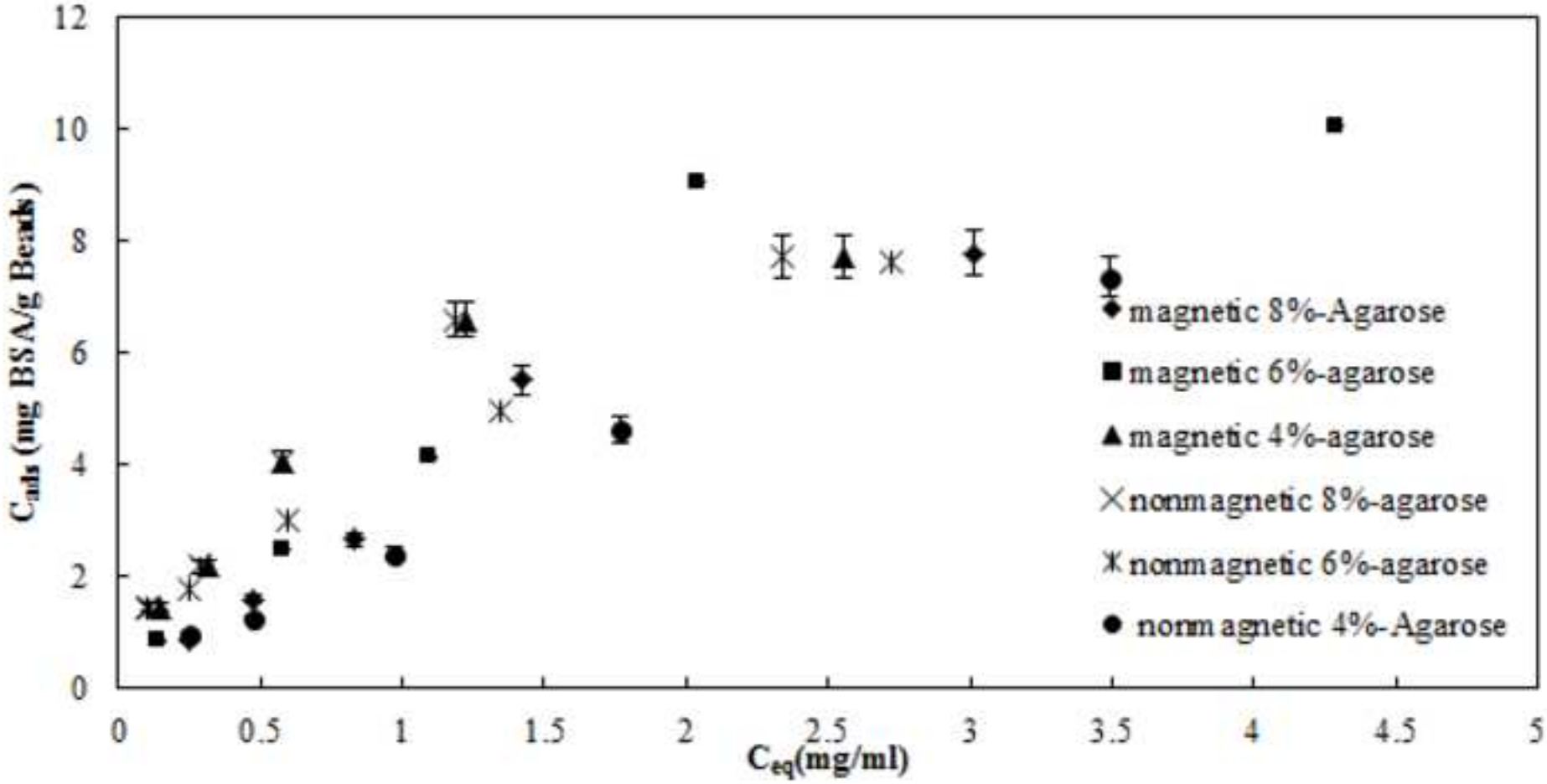
12
10
8
6
4
2
0
0
0.5
1
1.5
2
2.5
3
3.5
4
4.5
5
C_{ads} (mg BSA/g Beads)
C_{eq}(mg/ml)
magnetic 8%-Agarose
magnetic 6%-agarose
magnetic 4%-agarose
nonmagnetic 8%-agarose
nonmagnetic 6%-agarose
nonmagnetic 4%-Agarose

Figure 8

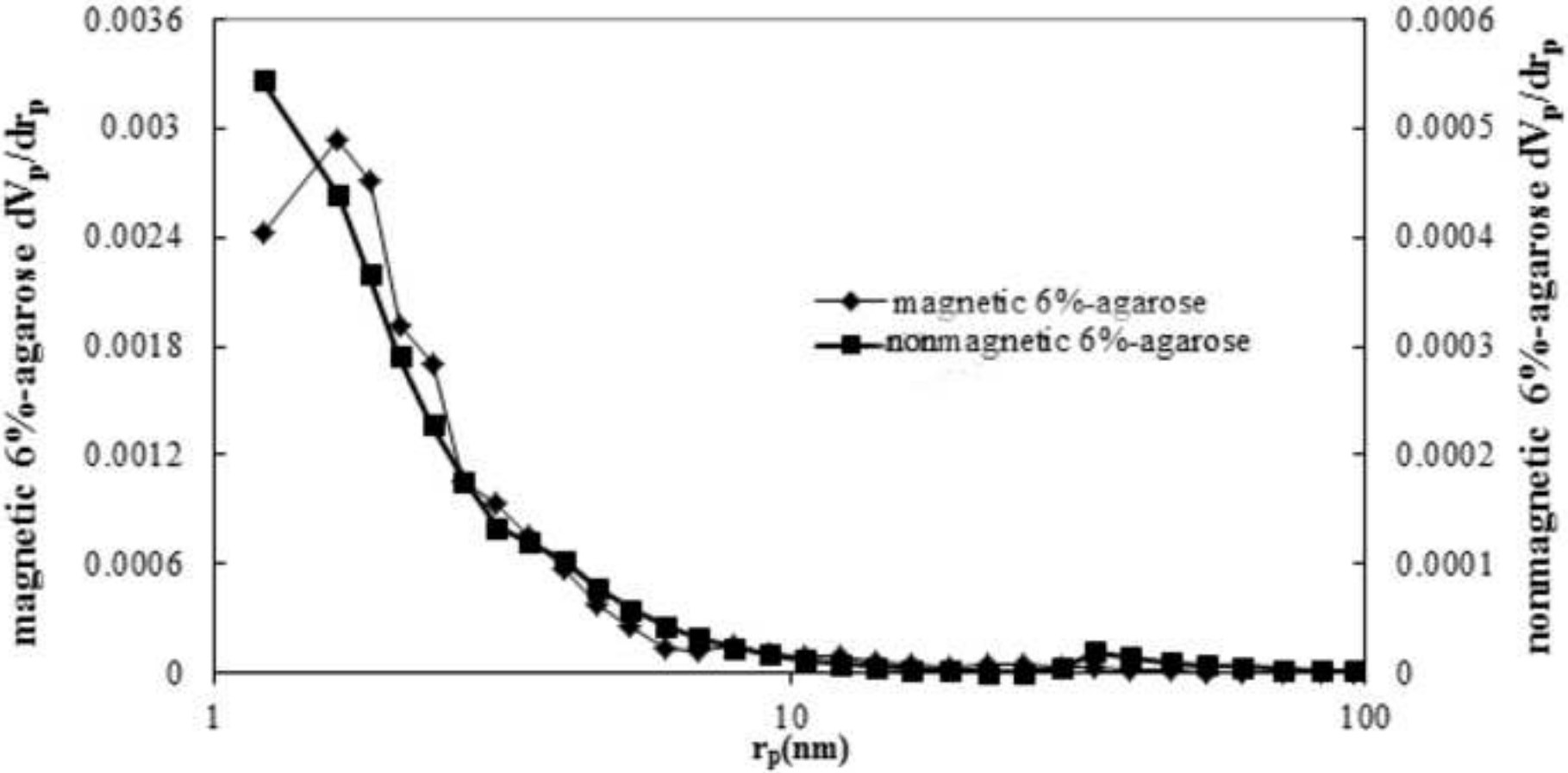
0.0036
0.003
0.0024
0.0018
0.0012
0.0006
0
magnetic 6%-agarose dV$_p$/dr$_p$
0.0006
0.0005
0.0004
0.0003
0.0002
0.0001
0
nonmagnetic 6%-agarose dV$_p$/dr$_p$
magnetic 6%-agarose
nonmagnetic 6%-agarose
1
10
100
r$_p$(nm)

Figure 9

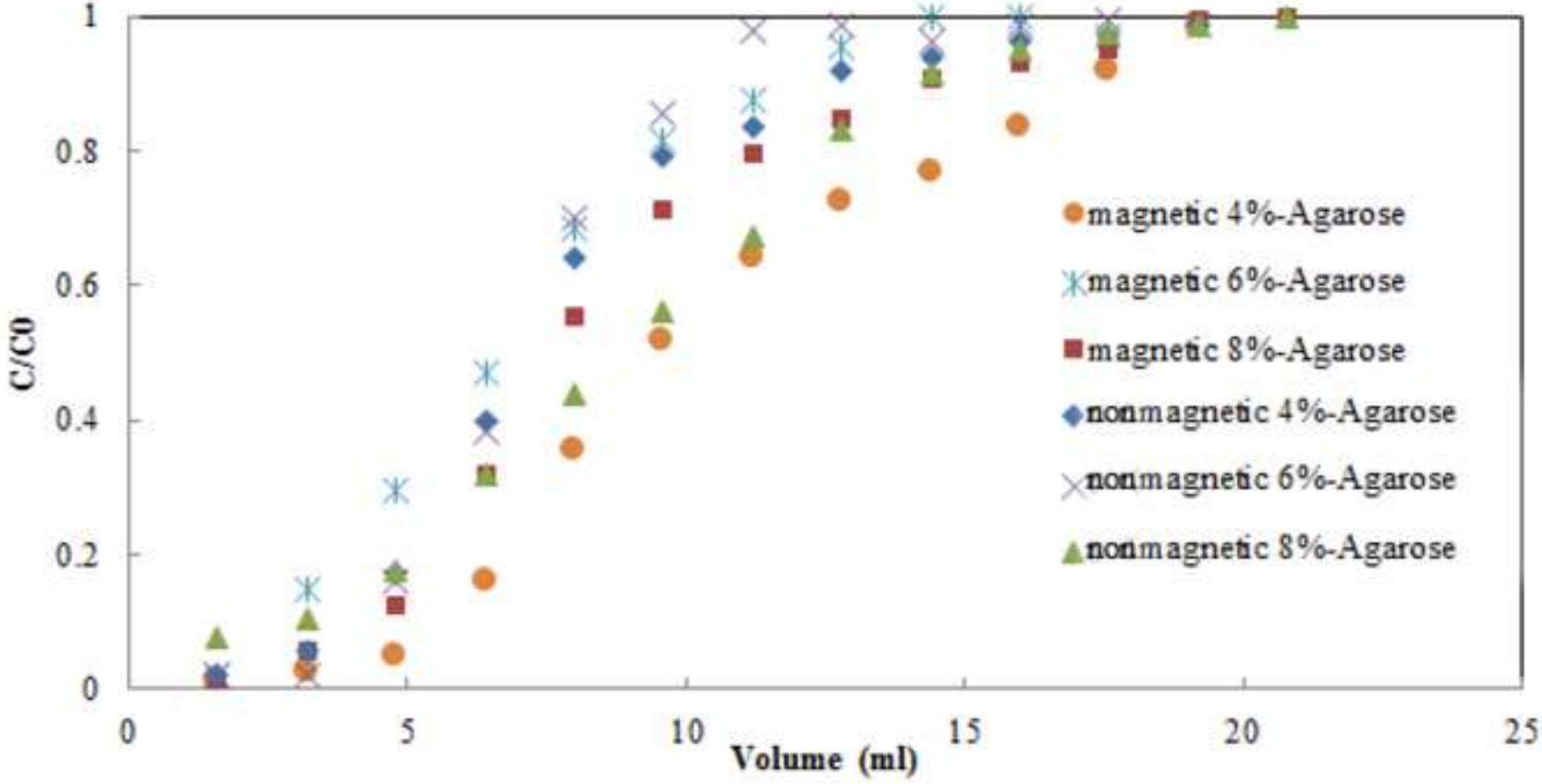
C/C0
Volume (ml)
0
0.2
0.4
0.6
0.8
1
0
5
10
15
20
25
magnetic 4%-Agarose
magnetic 6%-Agarose
magnetic 8%-Agarose
nonmagnetic 4%-Agarose
nonmagnetic 6%-Agarose
nonmagnetic 8%-Agarose

Figure 10

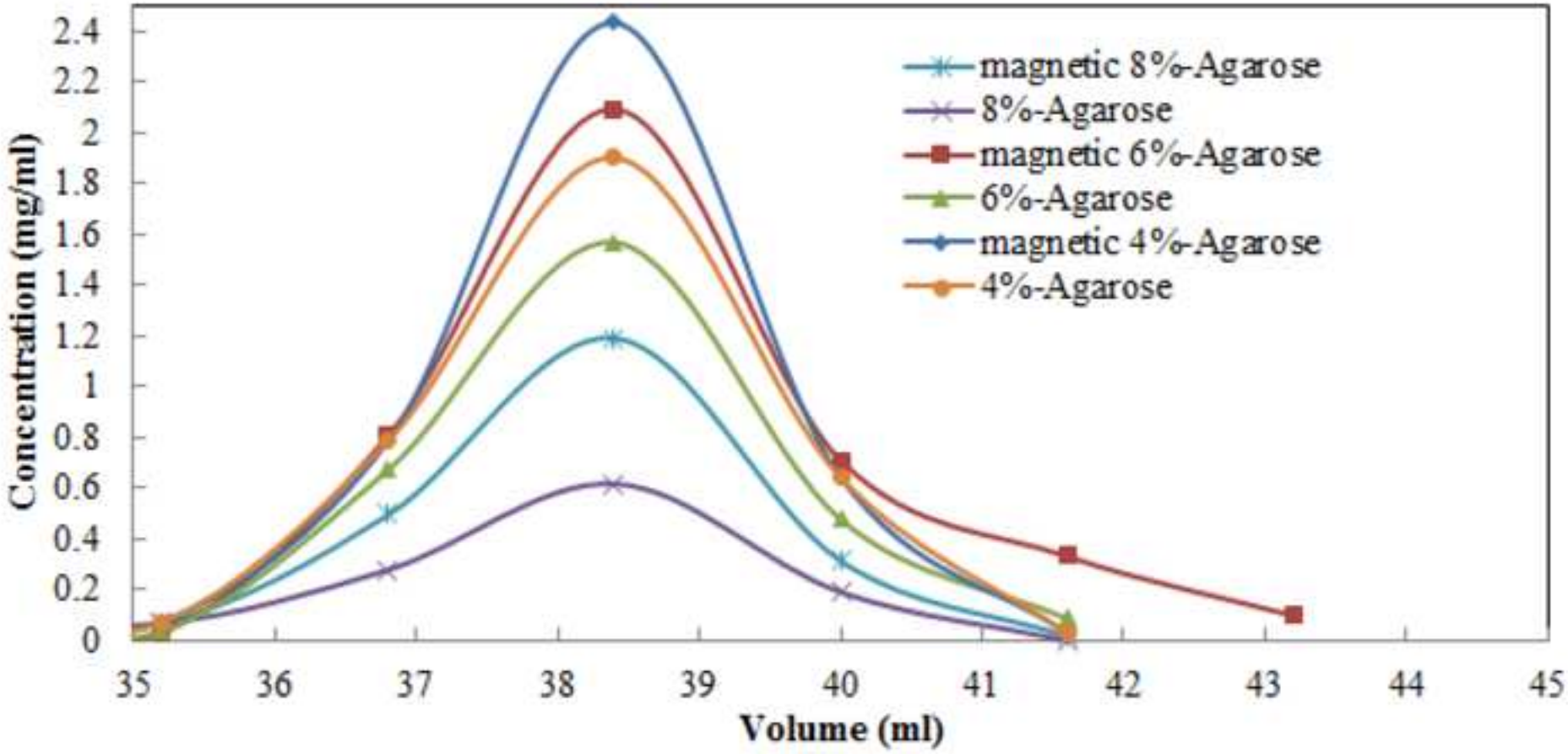
Concentration (mg/ml)
2.4
2.2
2
1.8
1.6
1.4
1.2
1
0.8
0.6
0.4
0.2
0
35
36
37
38
39
40
41
42
43
44
45
Volume (ml)
magnetic 8%-Agarose
8%-Agarose
magnetic 6%-Agarose
6%-Agarose
magnetic 4%-Agarose
4%-Agarose